Nano-Ionics与锂离子电池

陈立泉

中科院物理研究所

Lqchen@aphy.iphy.ac.cn

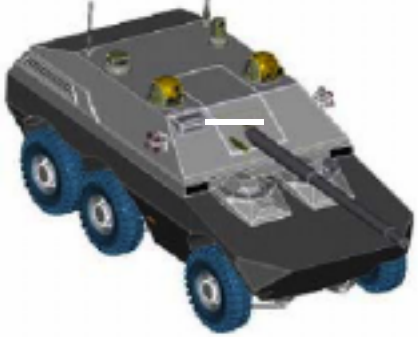

FIGURE 1-2 One version of the CHPS Notional Concept Vehicle. SOURCE of George Frazier, Science Applications International Corporation.

Address the key issues for emerging technologies in the development of the combat system components. The technologies to be addressed include permanent magnet t hub motors, Li-ion batteries, and high-temperature, wide band gap materials. Other

Sony回收约700万组笔记本锂离子电池

Solid State Ionics

- 主要研究对象：离子导体(Ionic conductor)或固体电解质(Solid State Electrolyte)，其电荷载流子是离子，而非电子。
- 发展到快离子导体(Superionic conductor 或Fast ionic conductor)，它们的离子电导率很高。
- 拓展到混合离子导体(Mixed Conductors)，其电荷载流子不仅是离子，还有电子。

从Solid State Ionics To Nano-Ionics

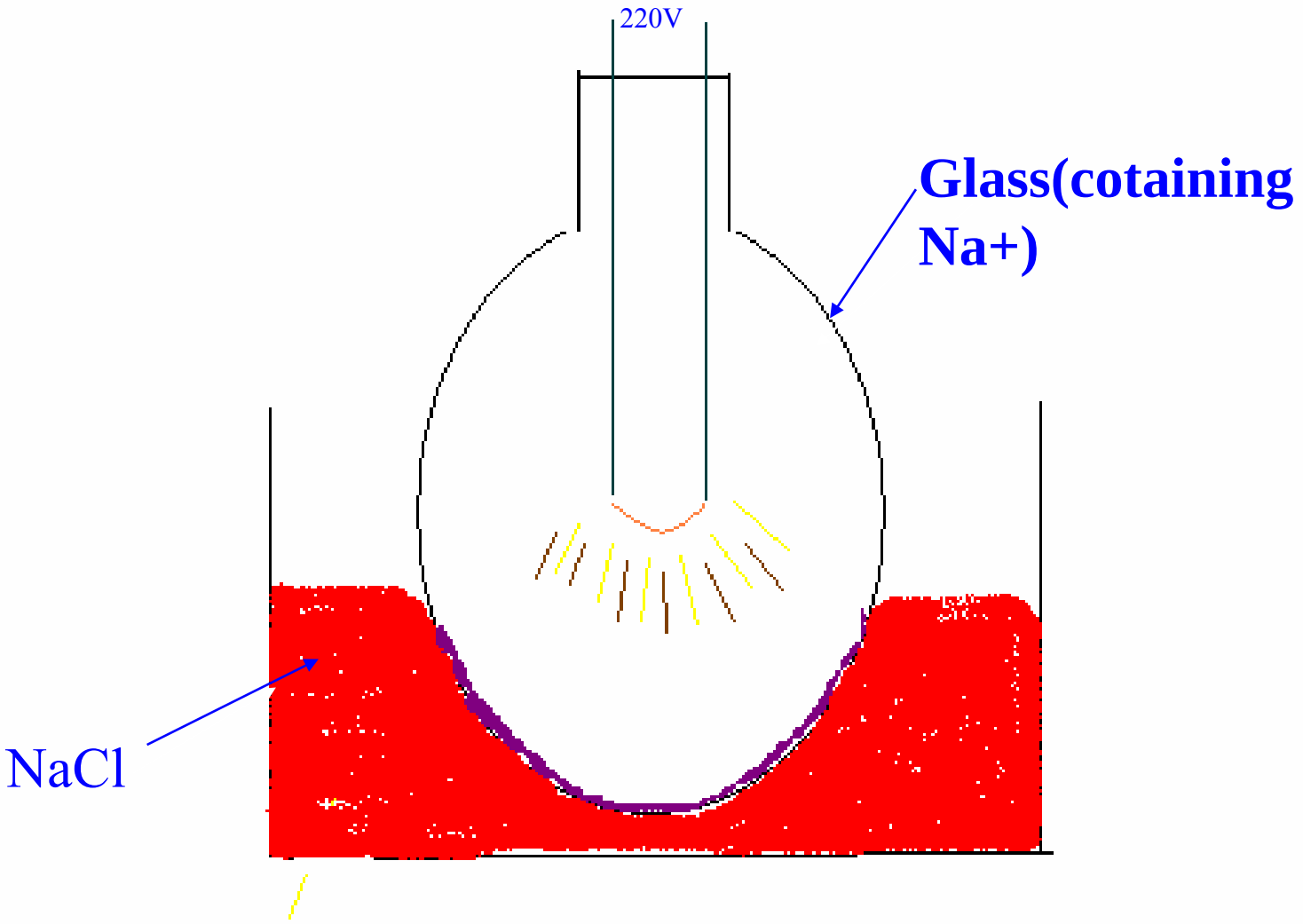
220V
Glass(cotaining Na+)
NaCl

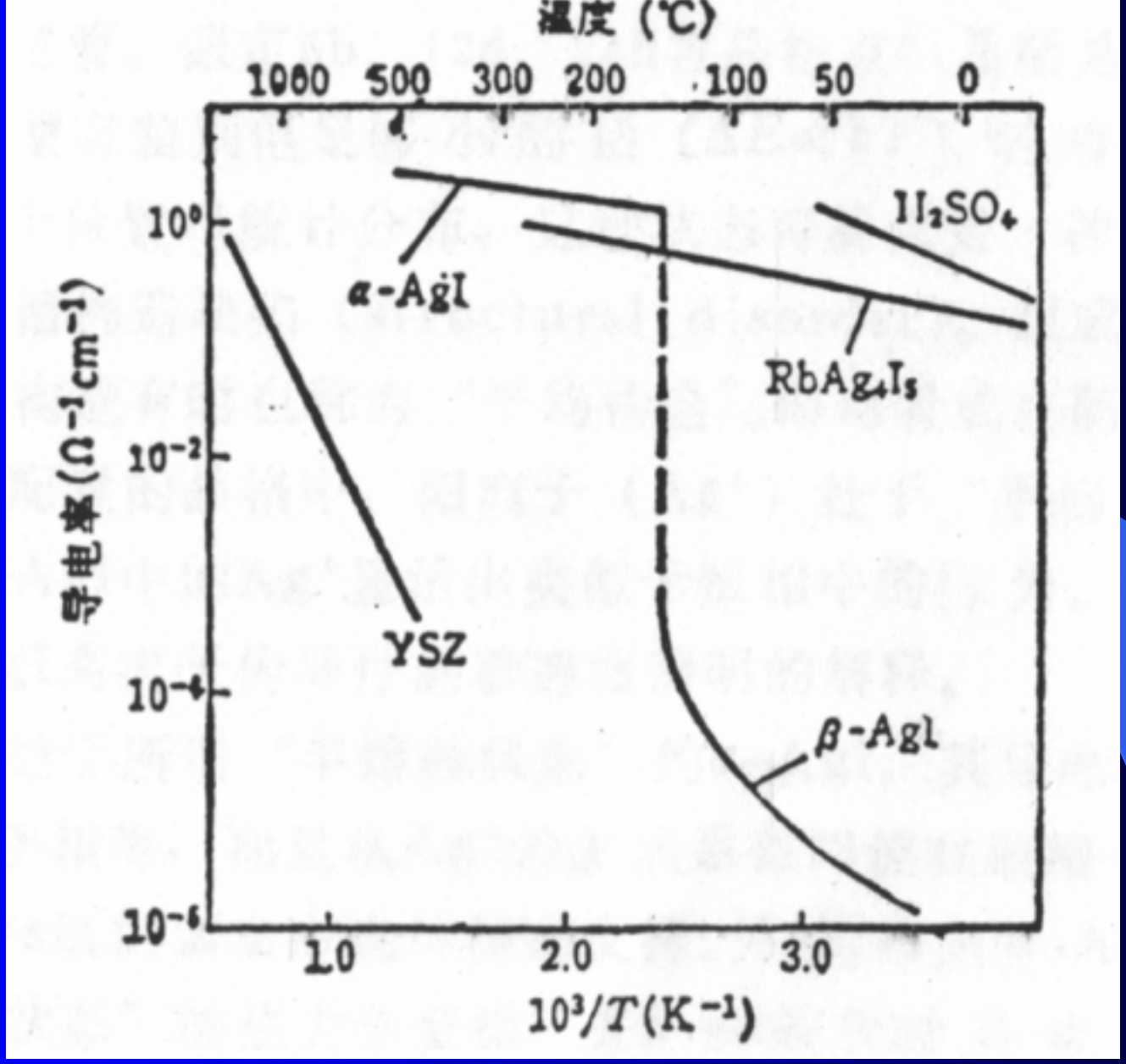

1913年Tubandt发现AgI在147C从 相转变到 相,电导率增加3个数量级以上,达

表6.6 AgI以及CuBr的相变温度和熵变值(ΔS_t, ΔS_m)

化合物	相变温度 (T_t/K)	ΔS_t/JK^{-1}mol^{-1}	熔点(T_m/K)	ΔS_m/JK^{-1}mol^{-1}
AgI	419	14.5	830	11.3
CuBr	664	9.0	761	12.6

〔M.O,Keefe *et al.*, *Philos, Mag.*,33, 220 (1976)〕

离子形成bcc晶格，

个Ag离子随机分布在

2个位置上：

6b(八面体)

12d(四面体)

24h(三角双锥)

结构是准熔态

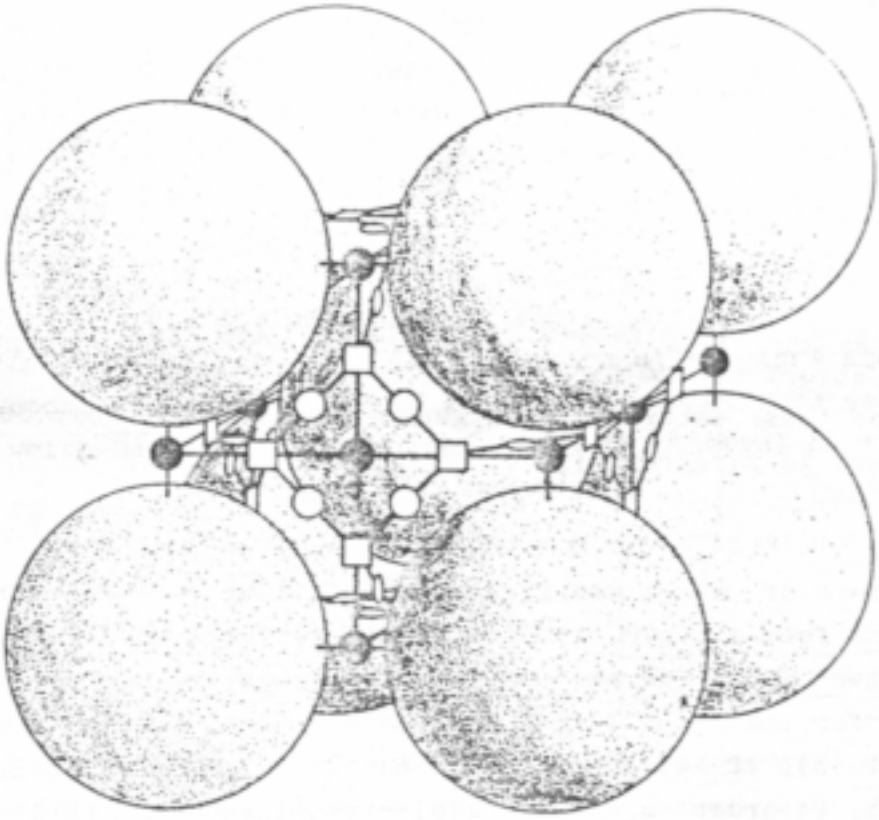

FIG. 8. Crystal structure of α-AgI according to Strock [7] and Hoshino [8]. The 6b sites are marked ●, the 12d sites are marked □, and the 24h sites are marked ○. The lattice constant is 5.06 Å at 250 °C [8].

中子衍射表明:
2个Ag离子位于四面体位(12d),
向八面体位(6b)延伸

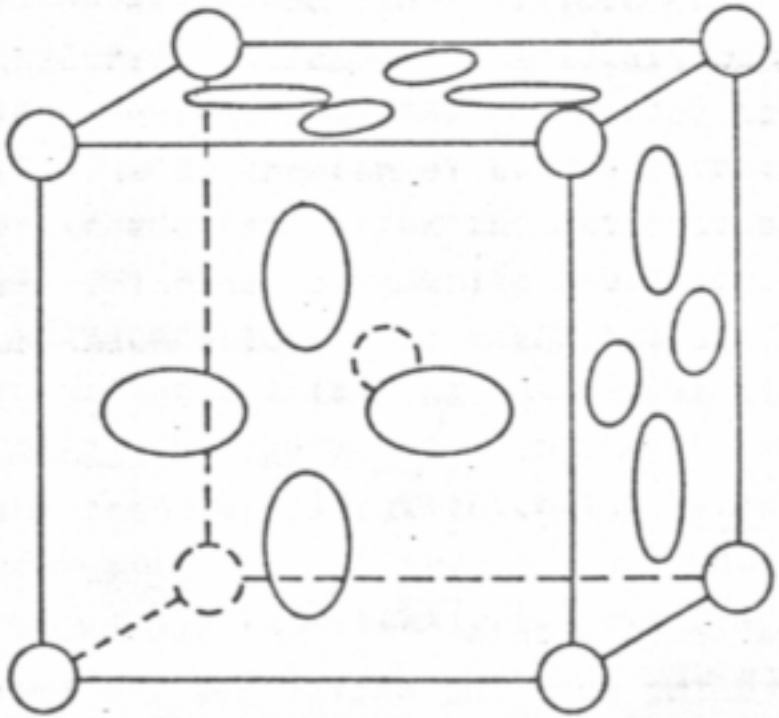

FIG. 9. Crystal structure of α-AgI according to Wright and Fender
The figure gives the positons and r.m.s. displacements of the nuclei at 200 °C.

Systems with $D \gtrsim 10^{-5}\,cm^2\,s^{-1}$

simple monoatomic liquids

α-Ag I
α-Cu I
β-CuBr
etc.

hydrogen in metals, e.g. H-Pd, H-Nb

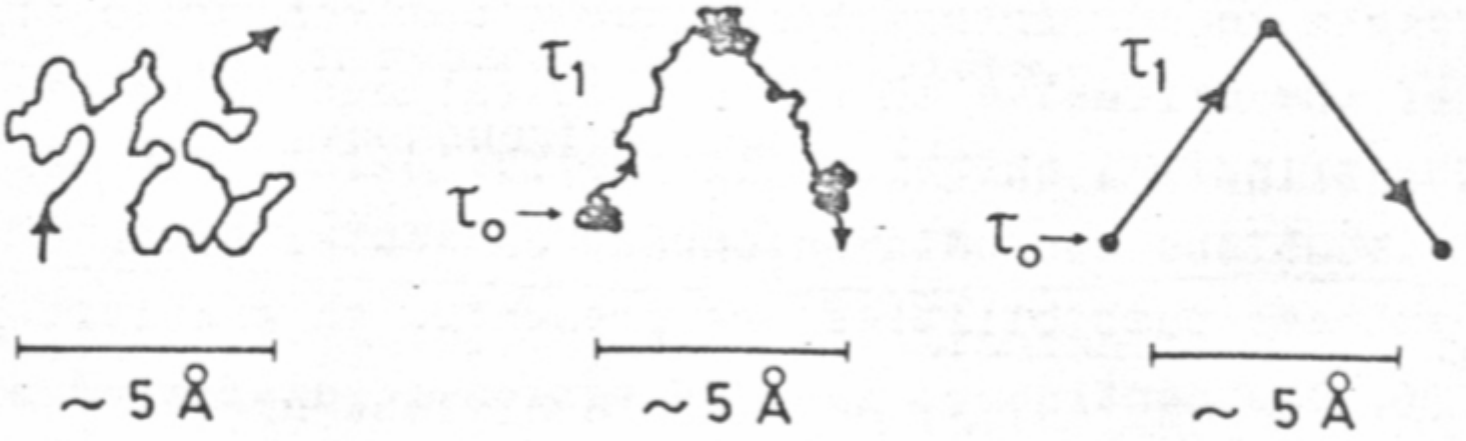

simple diffusion
$\tau_o = 0$

local motion
* jump diffusion
$\tau_o \approx \tau_1 \approx 10^{-11}$ s

jump diffusion
$\tau_1 \ll \tau_o \approx 10^{-11}$ s

FIG. 25. Diffusion in different systems.

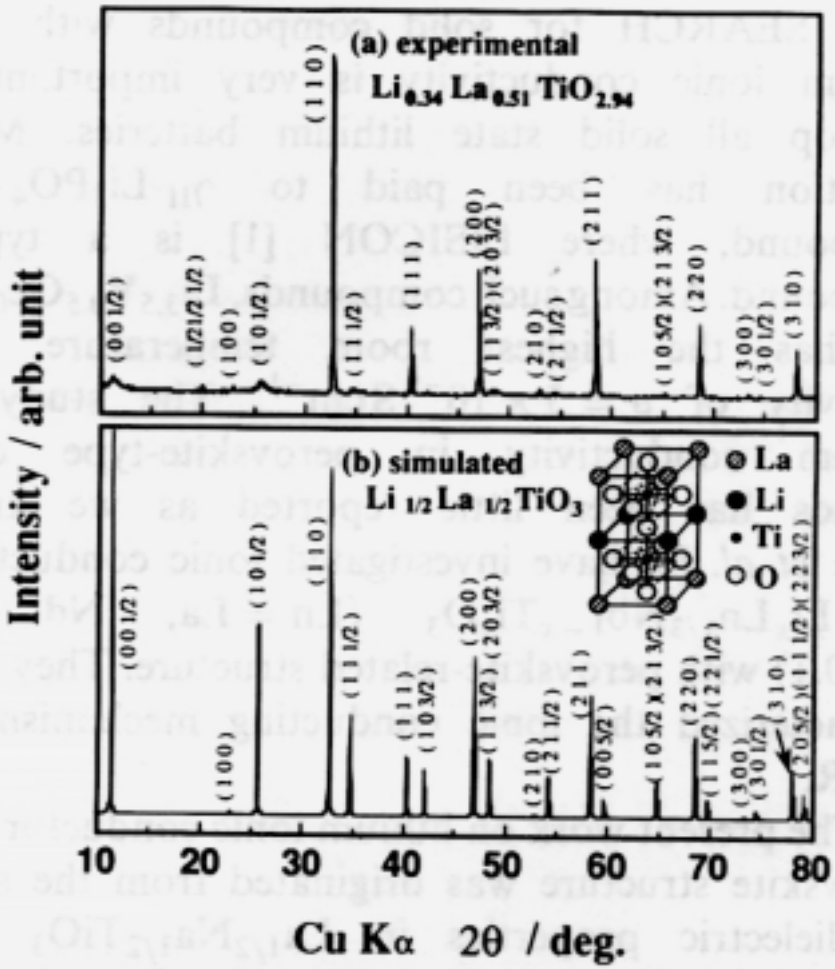

Fig. 1. (a) Powder X-ray diffraction pattern of $Li_{0.34(1)}La_{0.51(1)}TiO_{2.94(2)}$. (b) Simulated powder X-ray diffraction pattern and the crystal structure of $Li_{1/2}La_{1/2}TiO_3$ in which La and Li are perfectly ordered parallel to the *c*-axis.

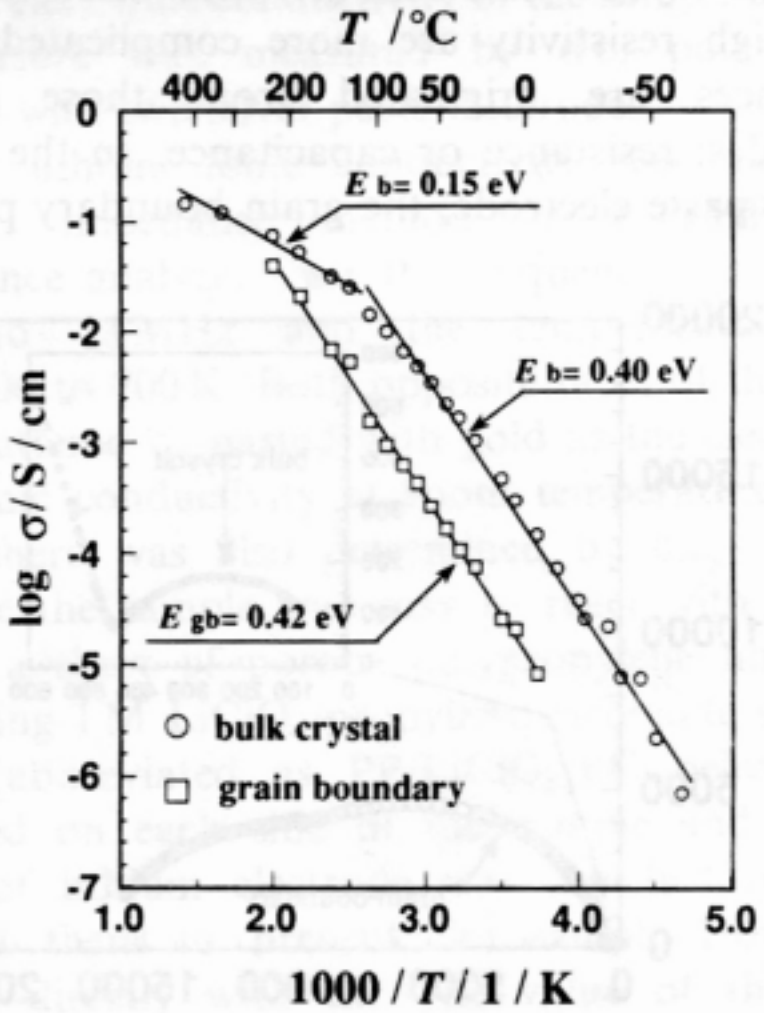

Fig. 5. Arrhenius plots of conductivity for $Li_{0.34(1)}La_{0.51(1)}TiO_{2.94(2)}$, circles: bulk crystal region, squares: grain boundary region.

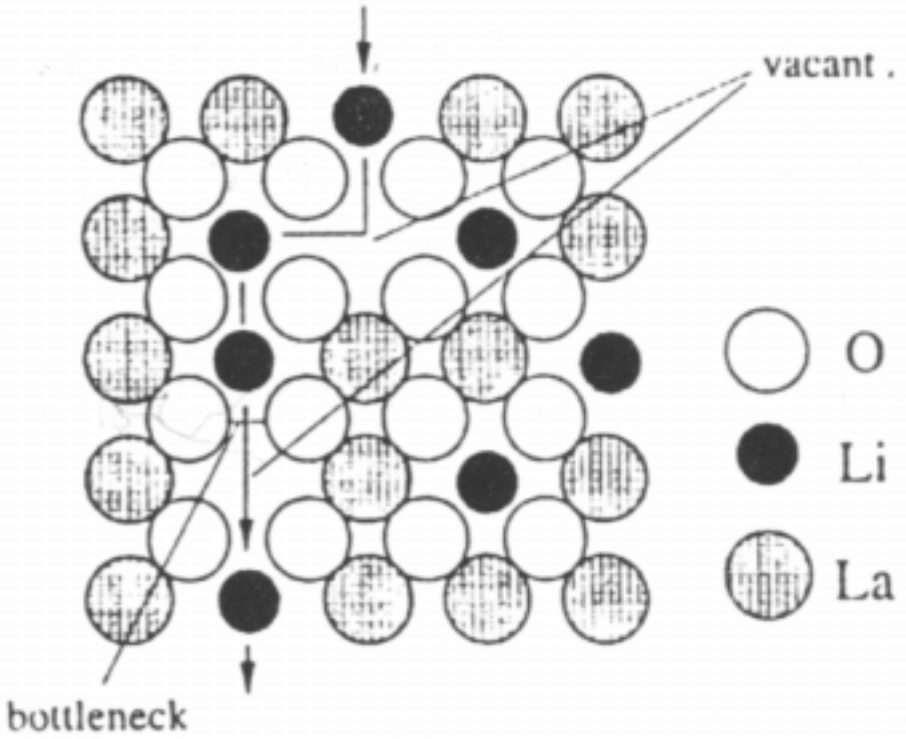

Fig.2 Arrangement of A-site ion and oxide ions, and lithium ion concentration in a perovskite-oxide.

快离子导体的判据

（1）晶体中必须存在一定数量活化能很低的可动离子，这些可动离子的尺寸应受到间隙位体积和开口处尺寸的限制。

（2）晶格中应包含能量近似相等，而数目远比传导离子数目为多的可容纳传导离子的间隙位，这些间隙位应具有出口，出口的线度应至少可与传导离子尺寸相比拟。

（3）可动离子可驻留的间隙位之间势垒不能太高，以使传导离子在间隙位之间可以比较容易跃迁。

（4）可容纳传导离子的间隙位应彼此互相连接，间隙位的分布应取共面多面体，构成一个立体间隙网络，其中拥有贯穿晶格始末的离子通道以传输可动离子。

良好的固体电解质材料应具有非常低的电子电导。

1. 晶格导电通道概貌

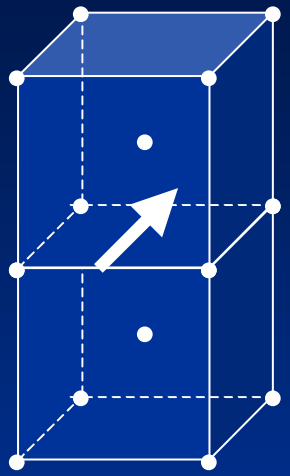

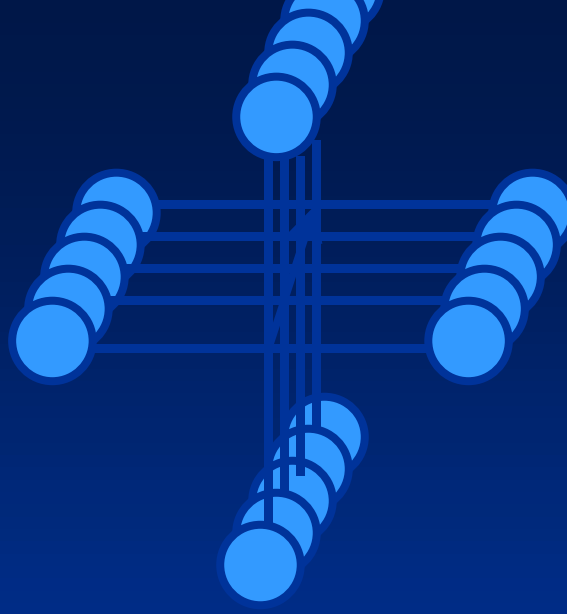

体心立方晶格导电通道

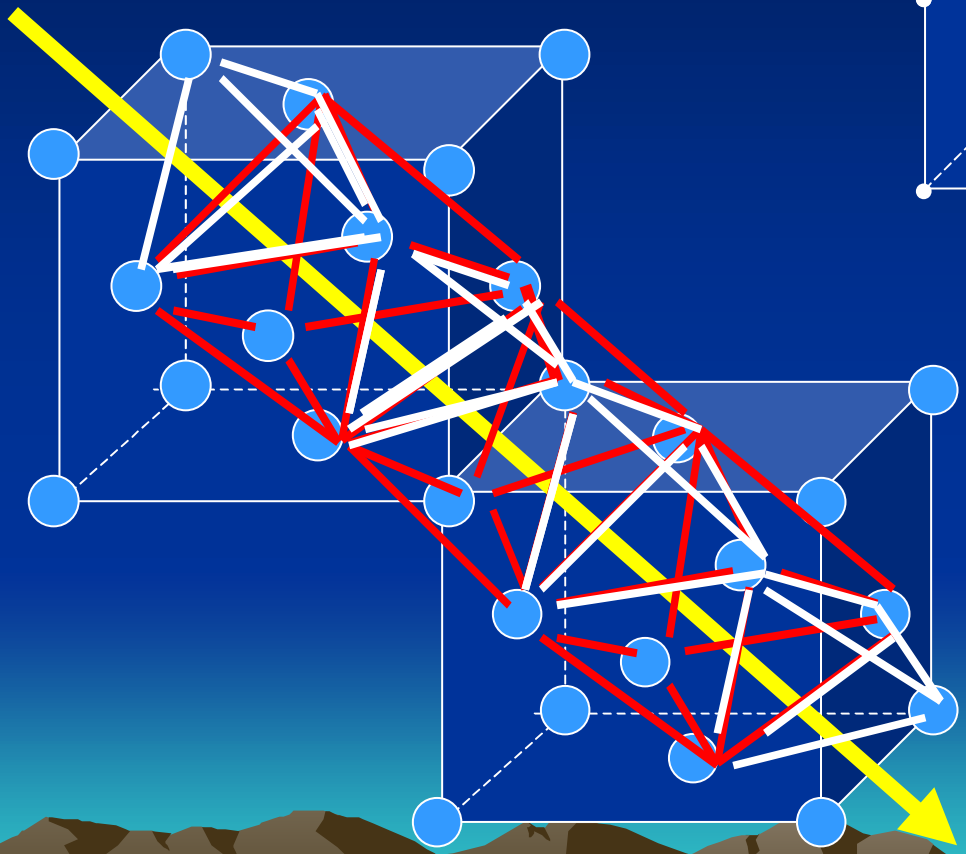

面心立方晶格导电通道

快离子导体的应用

燃料电池
电池
太阳能电池
传感器(气体/离子/生物)
电致变色
氧泵
电子器件

……

锂离子电池充电工作示意图

充电器

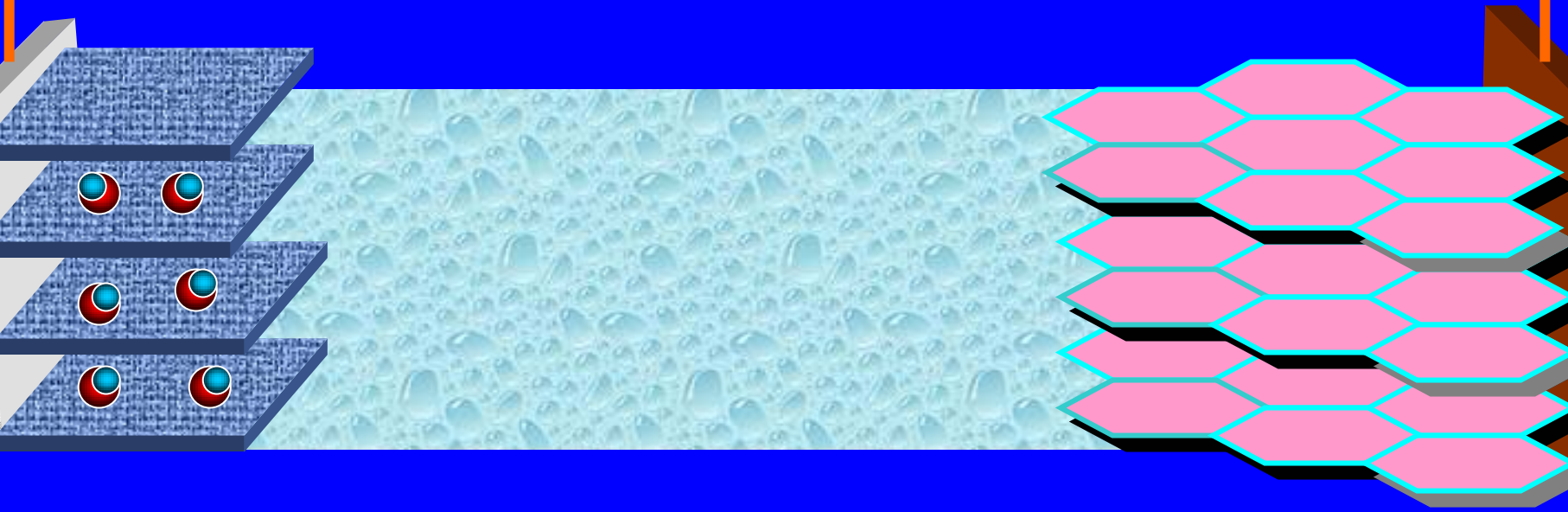

正　极	电解质溶液	负　极
$LiCoO_2$	$LiPF_6$/EC/DEC	C

锂离子电池充电工作示意图

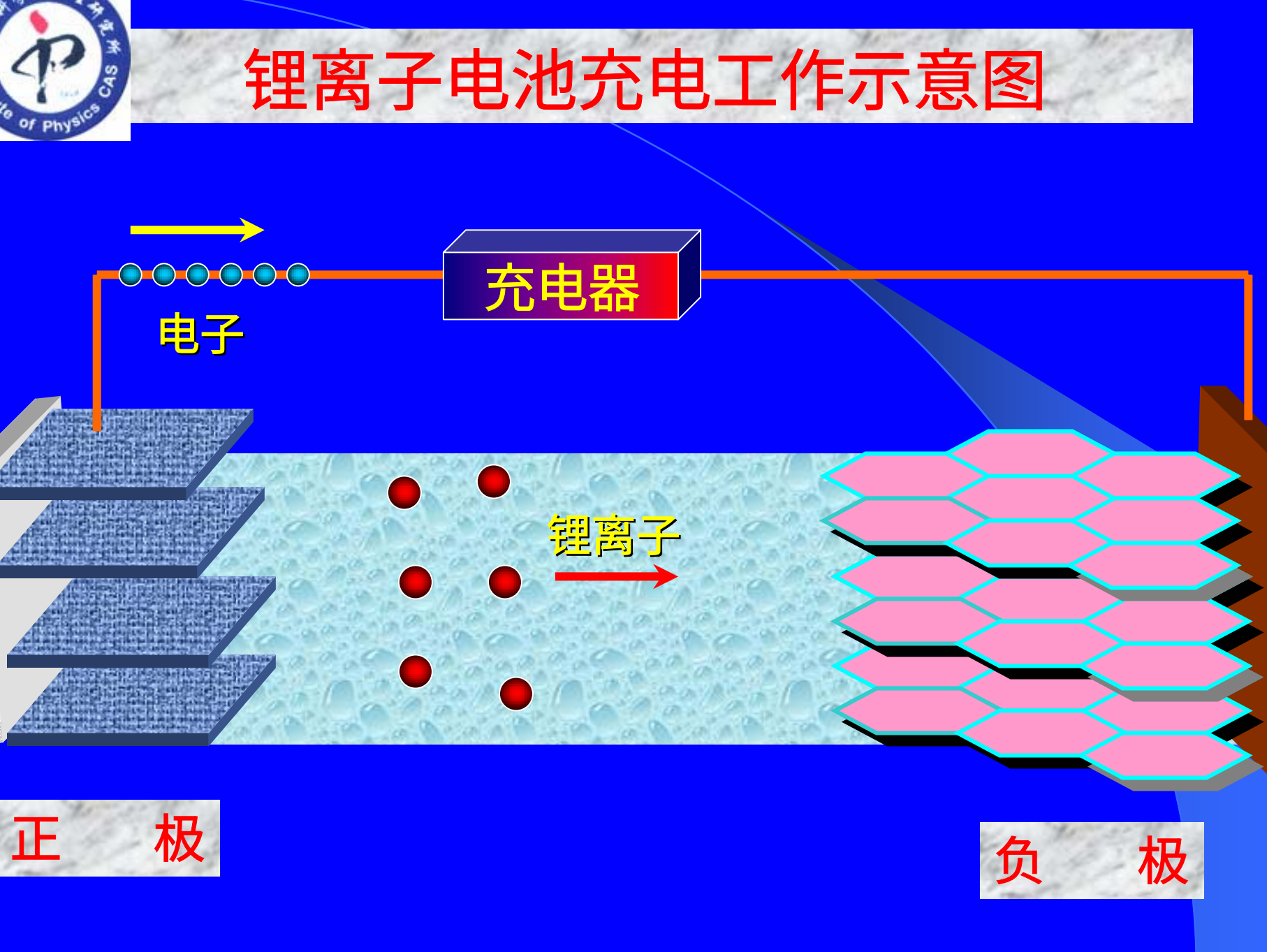

锂离子电池充电工作示意图

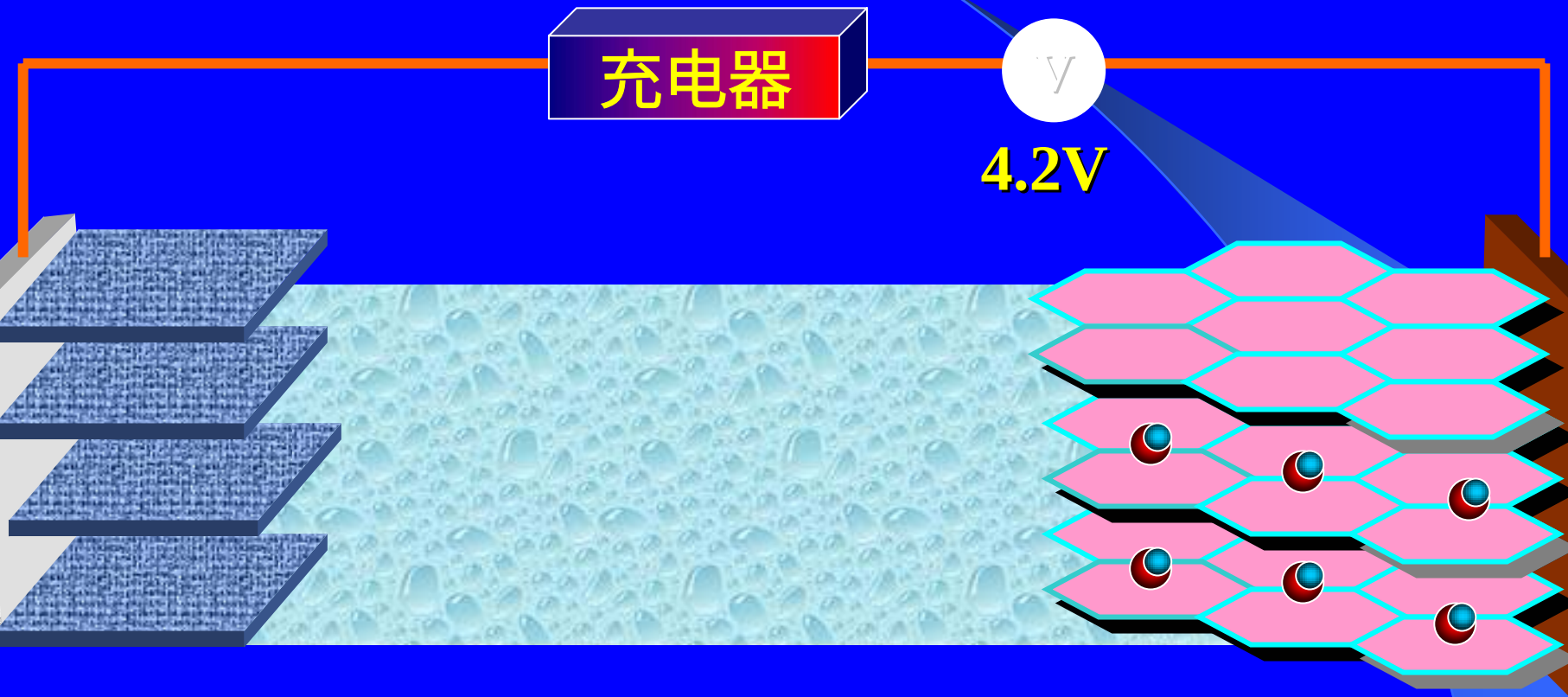

$C_6Li_x \rightleftharpoons C_{graphite} + x\,Li^+ + x\,e^-$

charge

Intercalation in graphite

Single-atom thick graphite layers. Interlayer distance 3.35Å (0.335nm)

Intercalation of:
lithium: 3.71Å
potassium: 5.35Å
AsF5: 8.15Å
KHg: 10.22 Å (three layers of K and Hg)

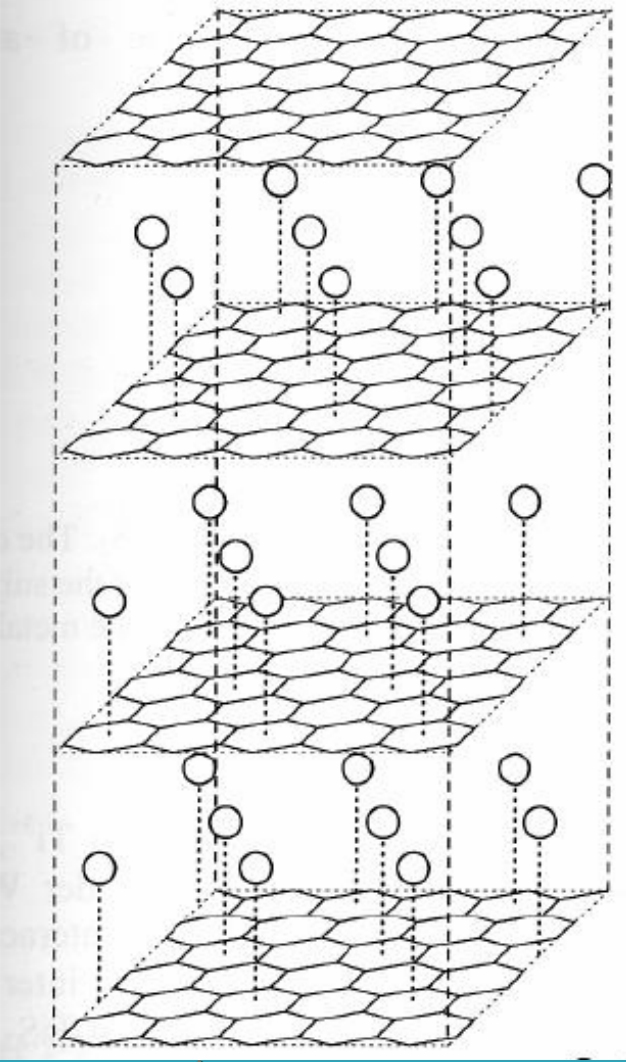

离子电子混合导体

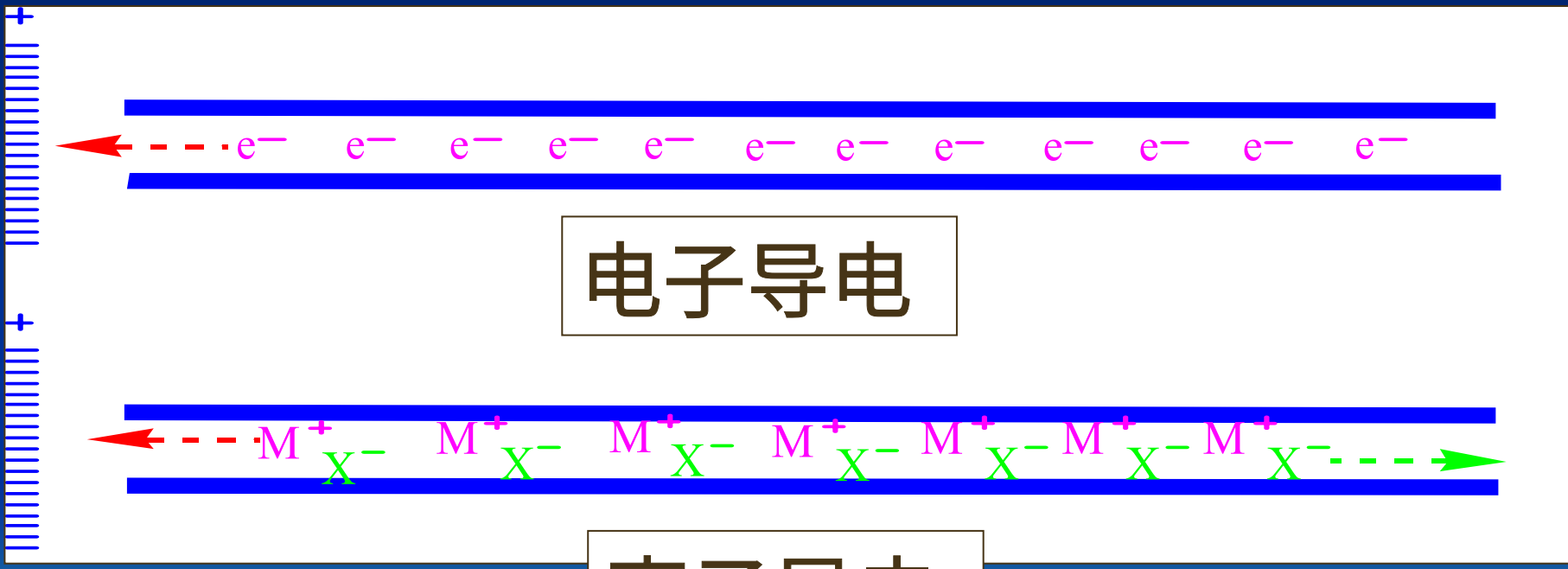

Doubled energy density in 10 years

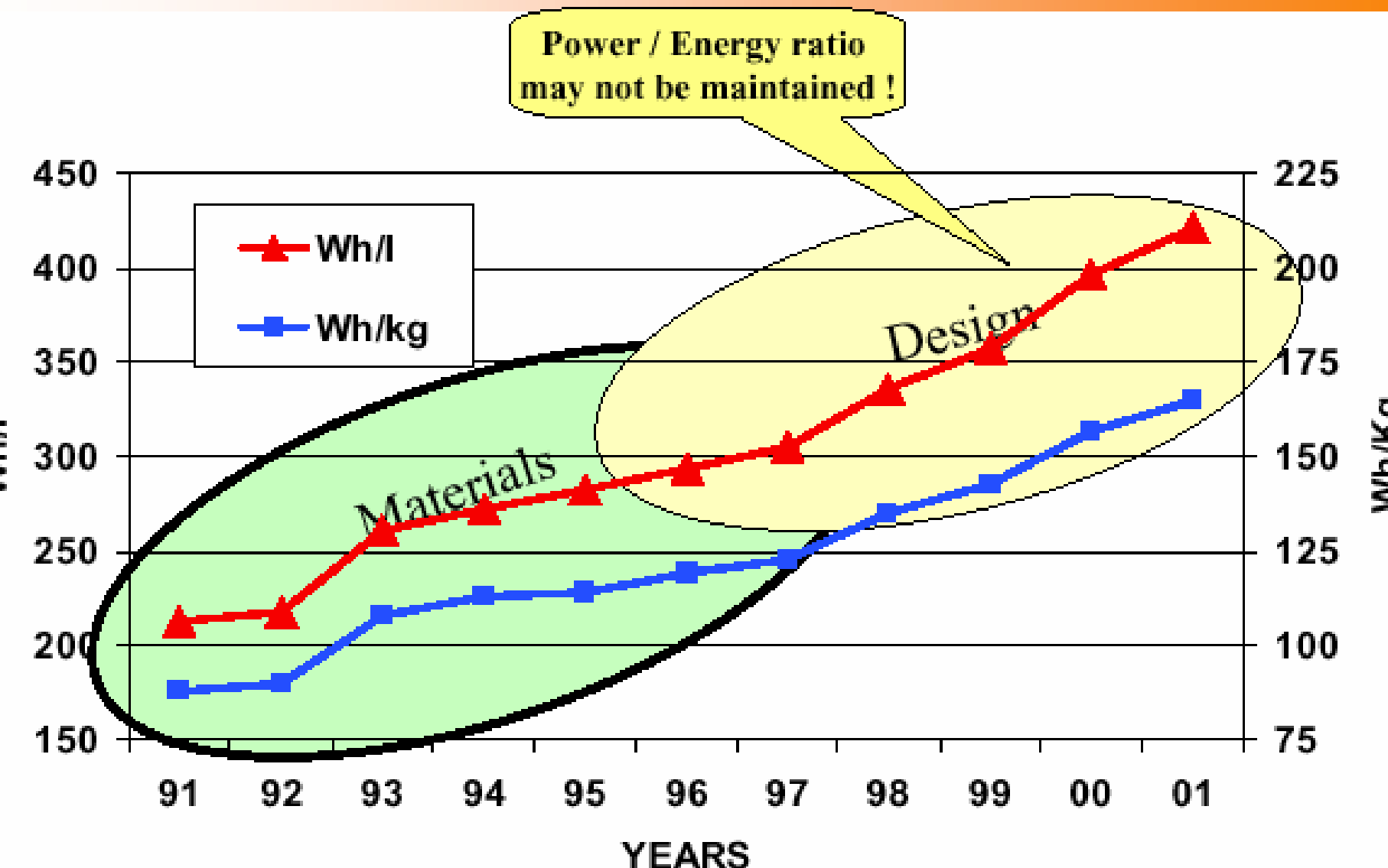

Evolution of energy for different battery technologies:

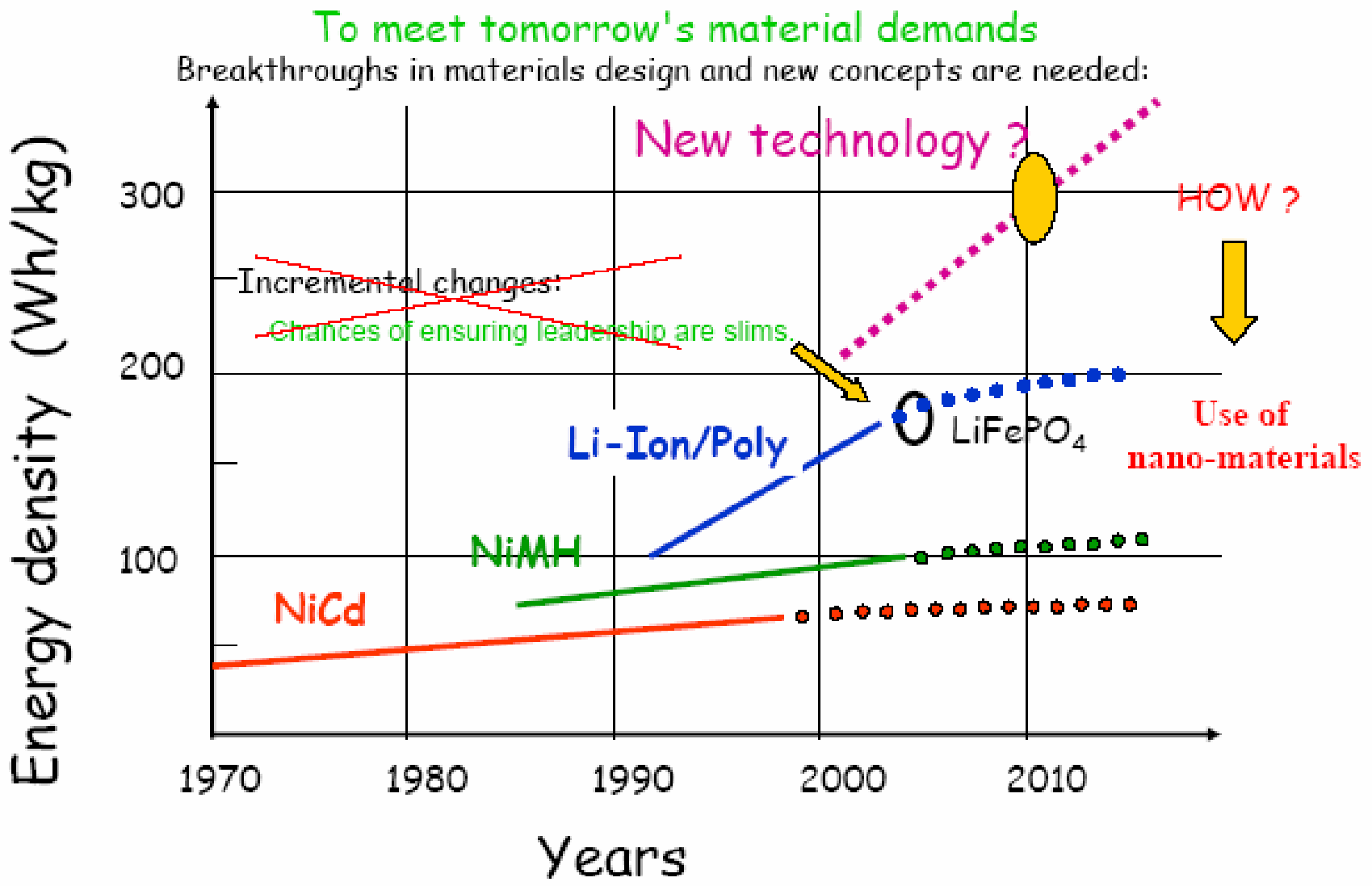

Data taken from:
J. Moller Nokia Mobile Phones, Fort Lauderdale, FB, March 2000.

Nano-Ionics?

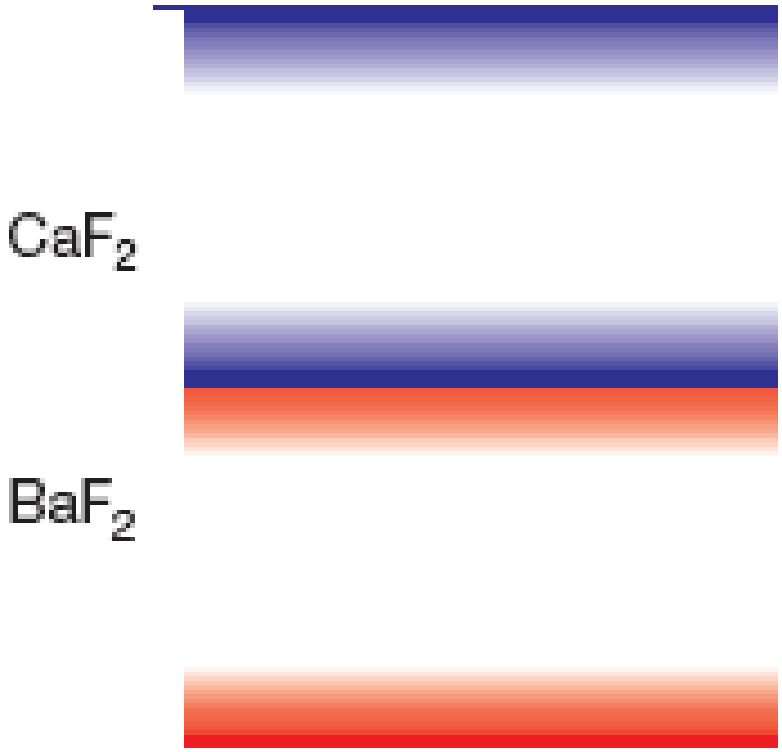

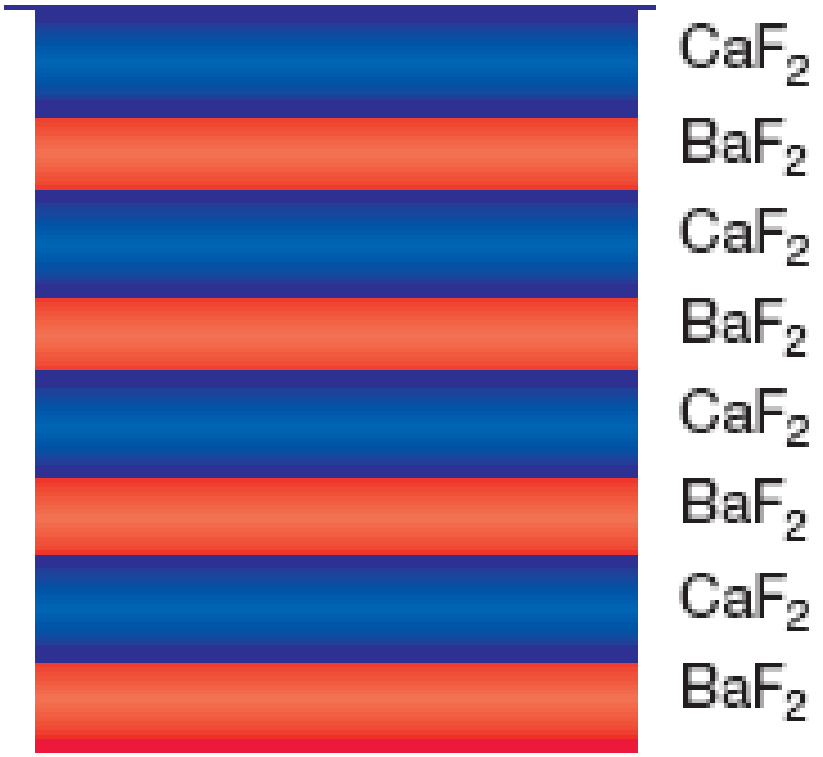

J. Maier etal

NATURE |VOL 408 | 21/28 DECEMBER 2000

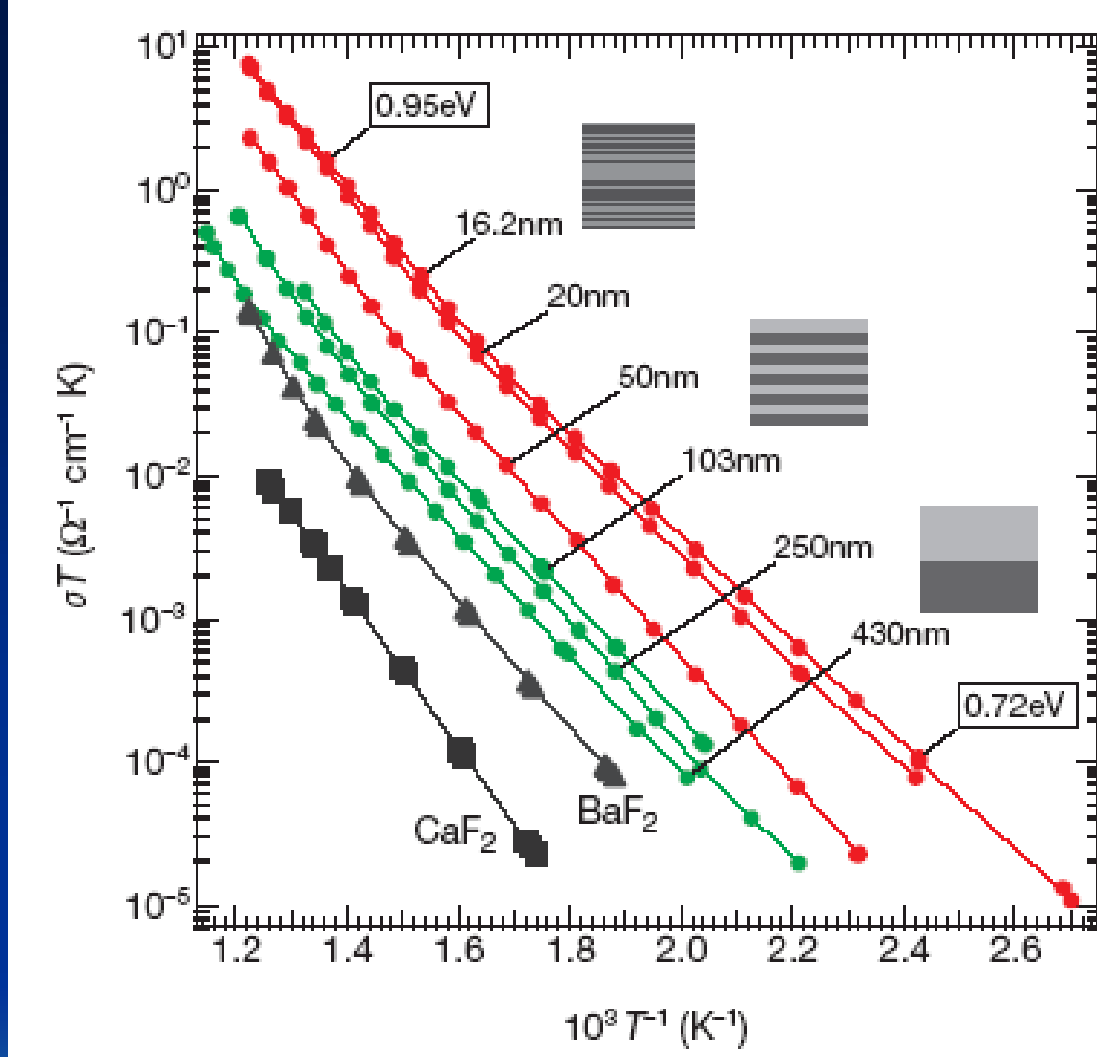

J. Maier etal

ATURE |VOL 408 | 21/28 DECEMBER 2000

Nanosized Li-Sn grains dispersed in amorphous Li_2O in discharged nano-SnO anode for Li ion batteries

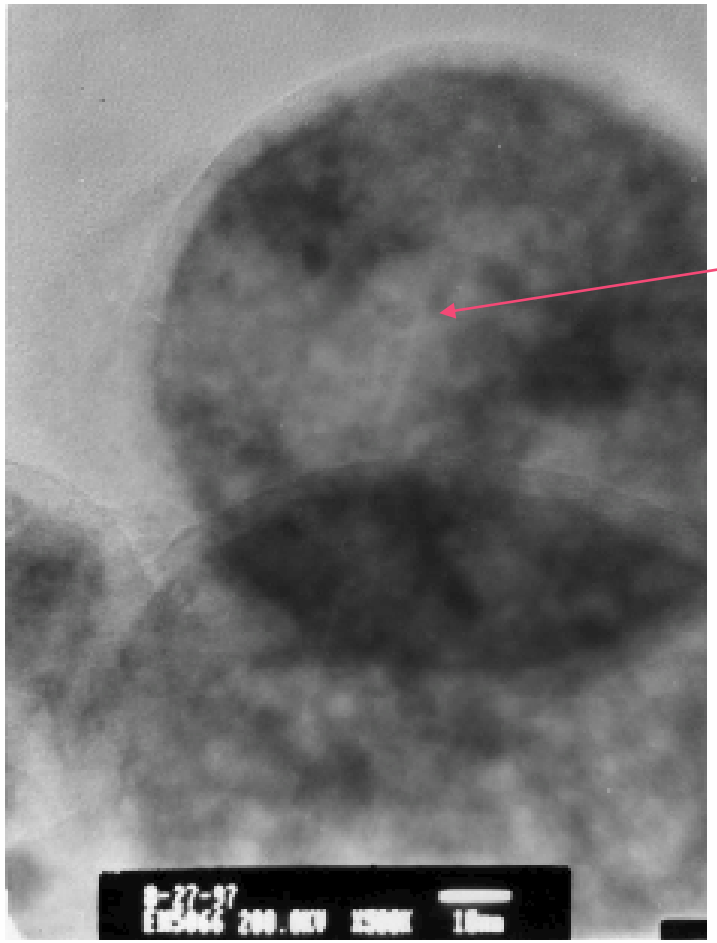

Figure 3. HRTEM image of nanometer-scale SnO particles after discharge to 0.0 V. A surface film can be seen on each particle. The particle size is 100 nm.

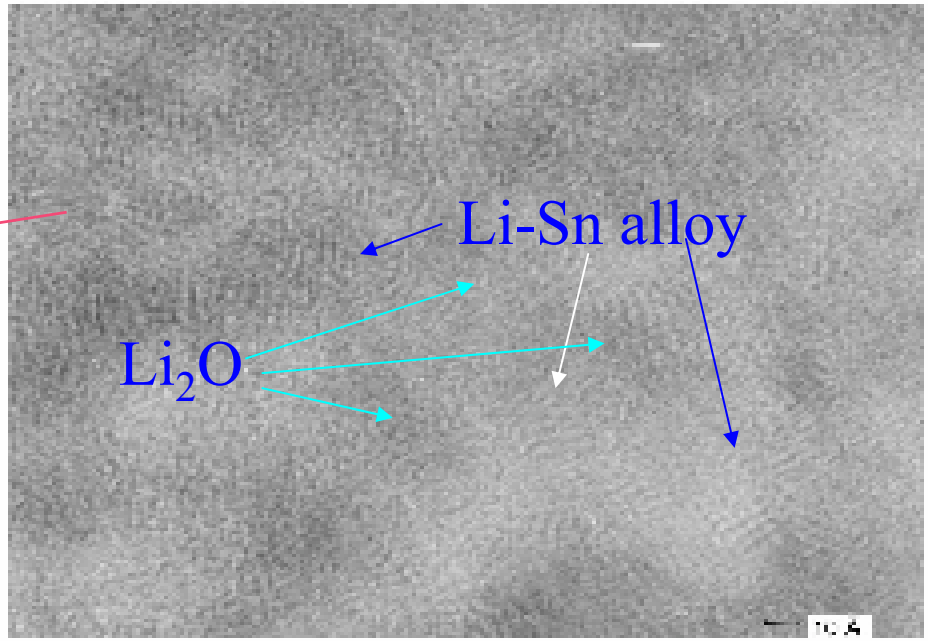

Figure 5. A typical HRTEM image of nanometer-scale SnO after discharg to 0.0 V. The selected area is in the core region of the same particle in Fig. 3

H. Li, X. J.Huang, L. Q. Chen, *Electrochem. and Solid-state Lett.* **1**, 241(1998)

The influence of particle size, content of CB, voltage limitation on the cyclic performance of Si-based anodes for secondary lithium batteries

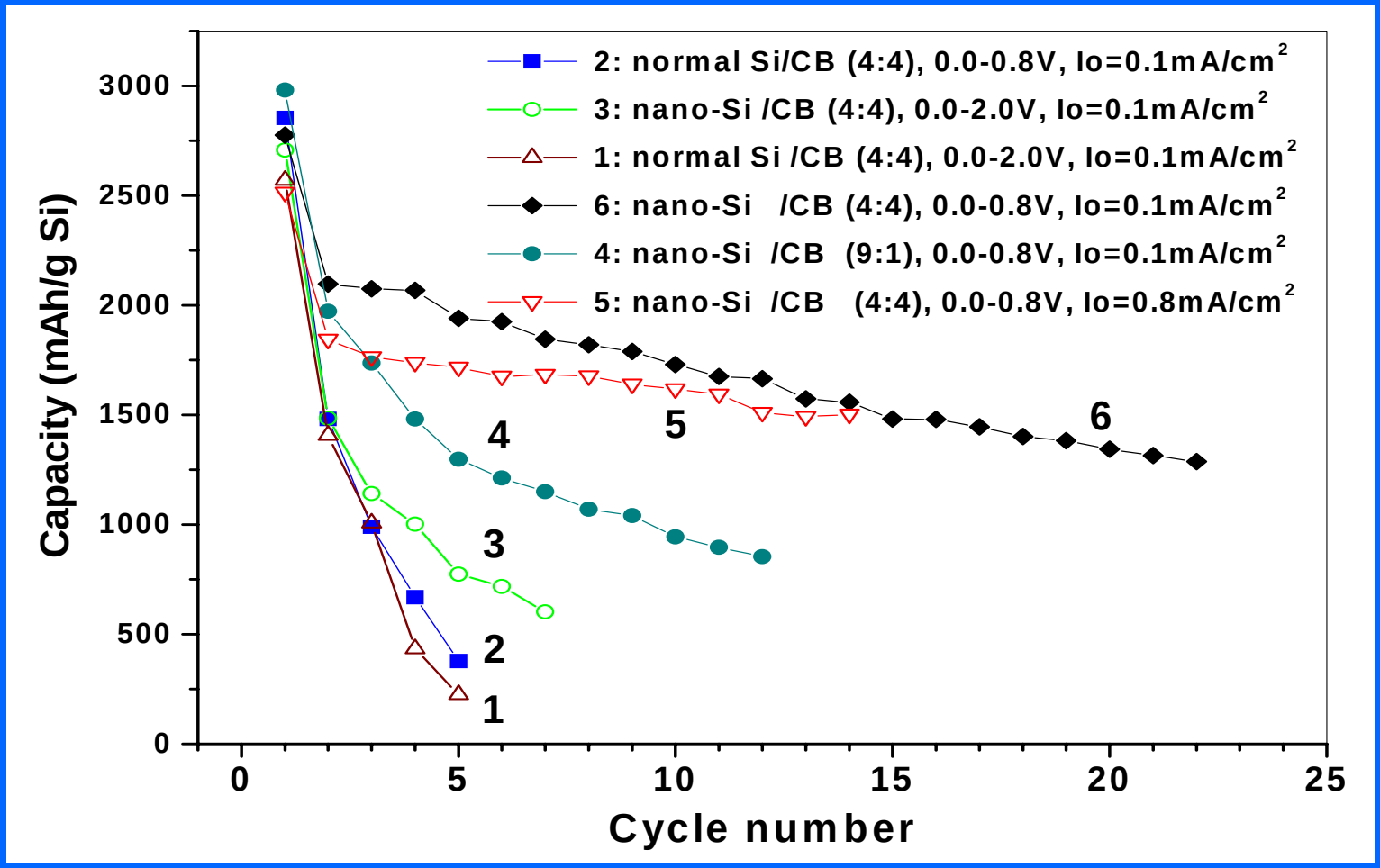

SAED patterns of Si nanoparticles at different Li-doping levels

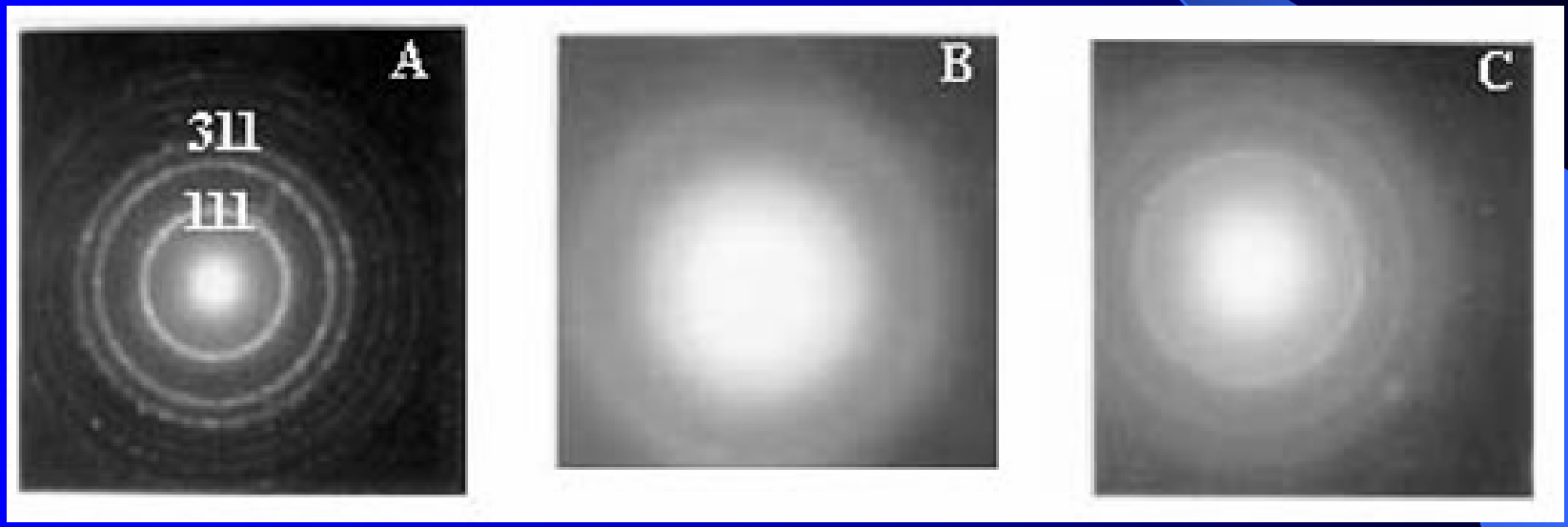

Original Nano-Si Heavy Li-doped Partly Li-extraction

Nano-SnSb on hard carbon spheres

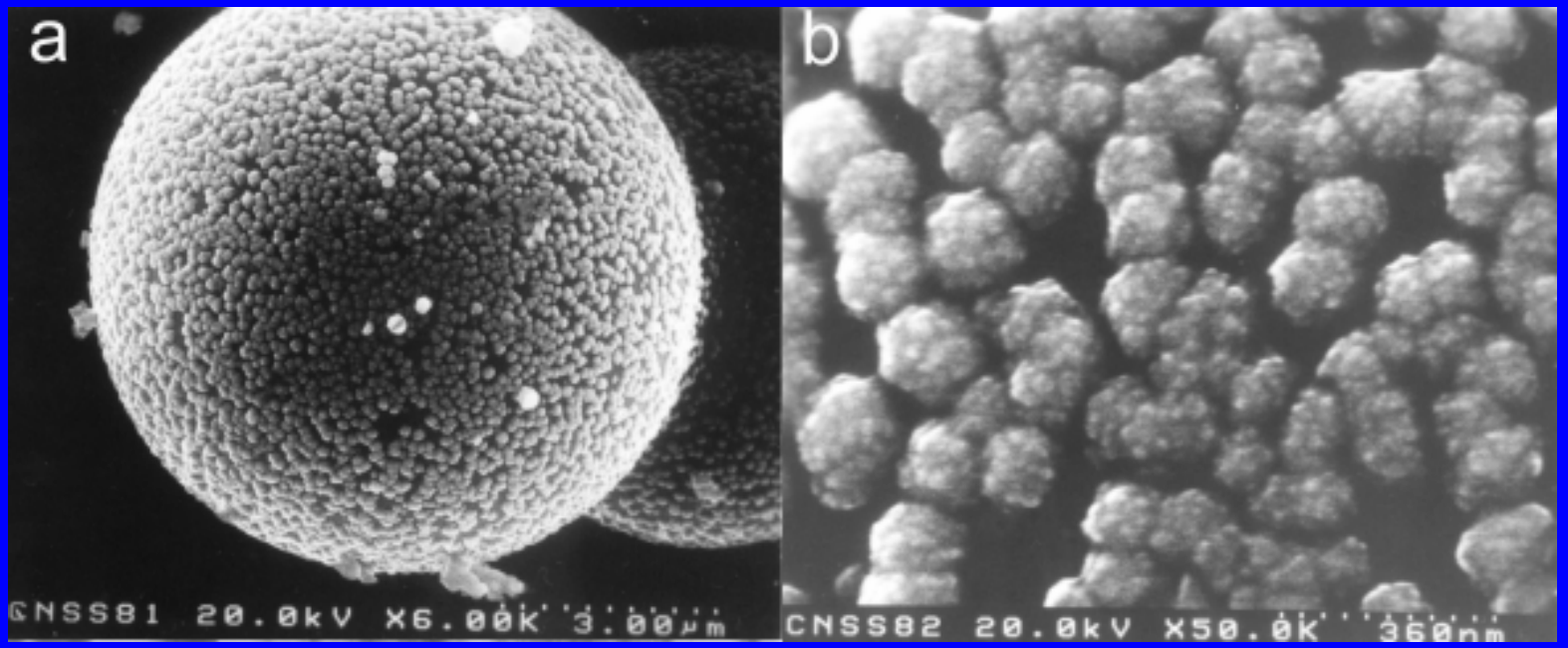

Morphology of 30wt% nano-SnSb alloy on hard carbon after Li ions insertion and extraction

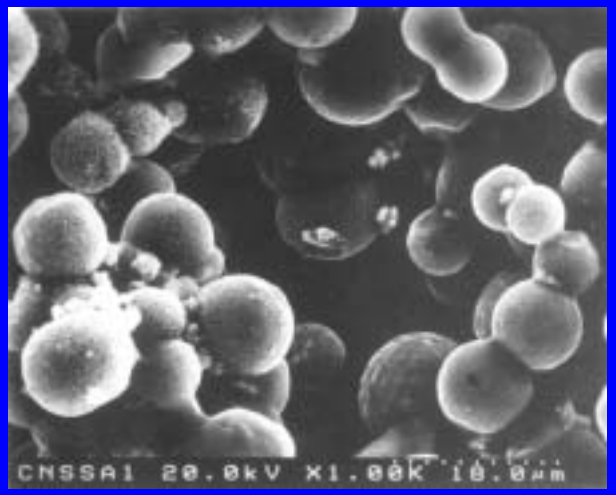

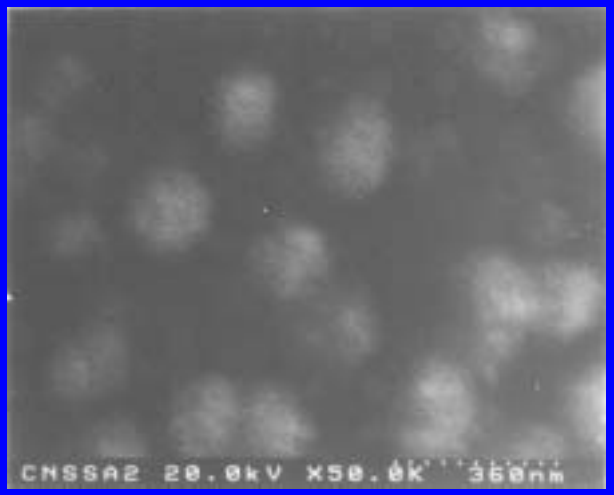

Li ions insertion

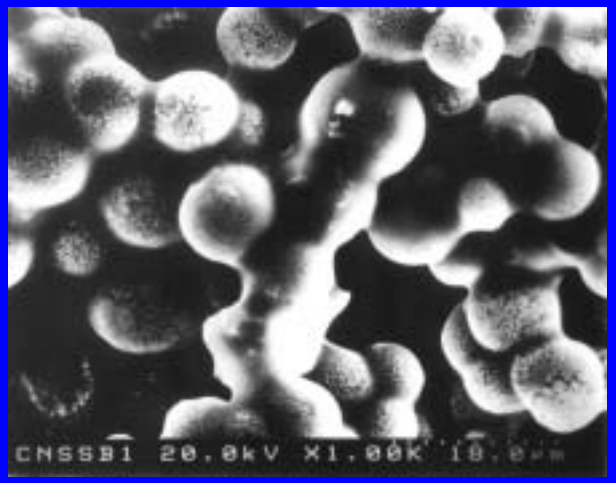

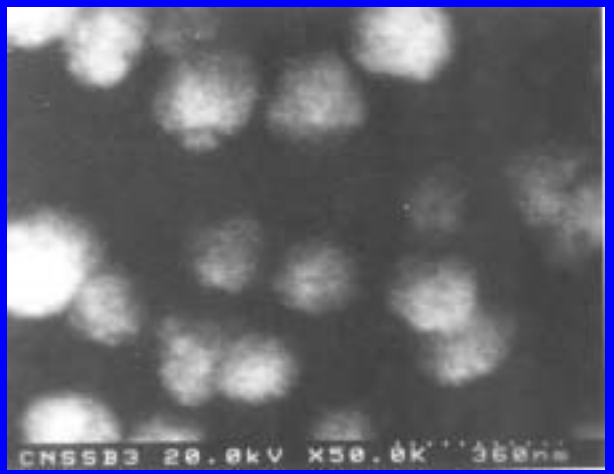

Li ions extraction

Microstructure of HCS coated by nanosized SnSb alloy

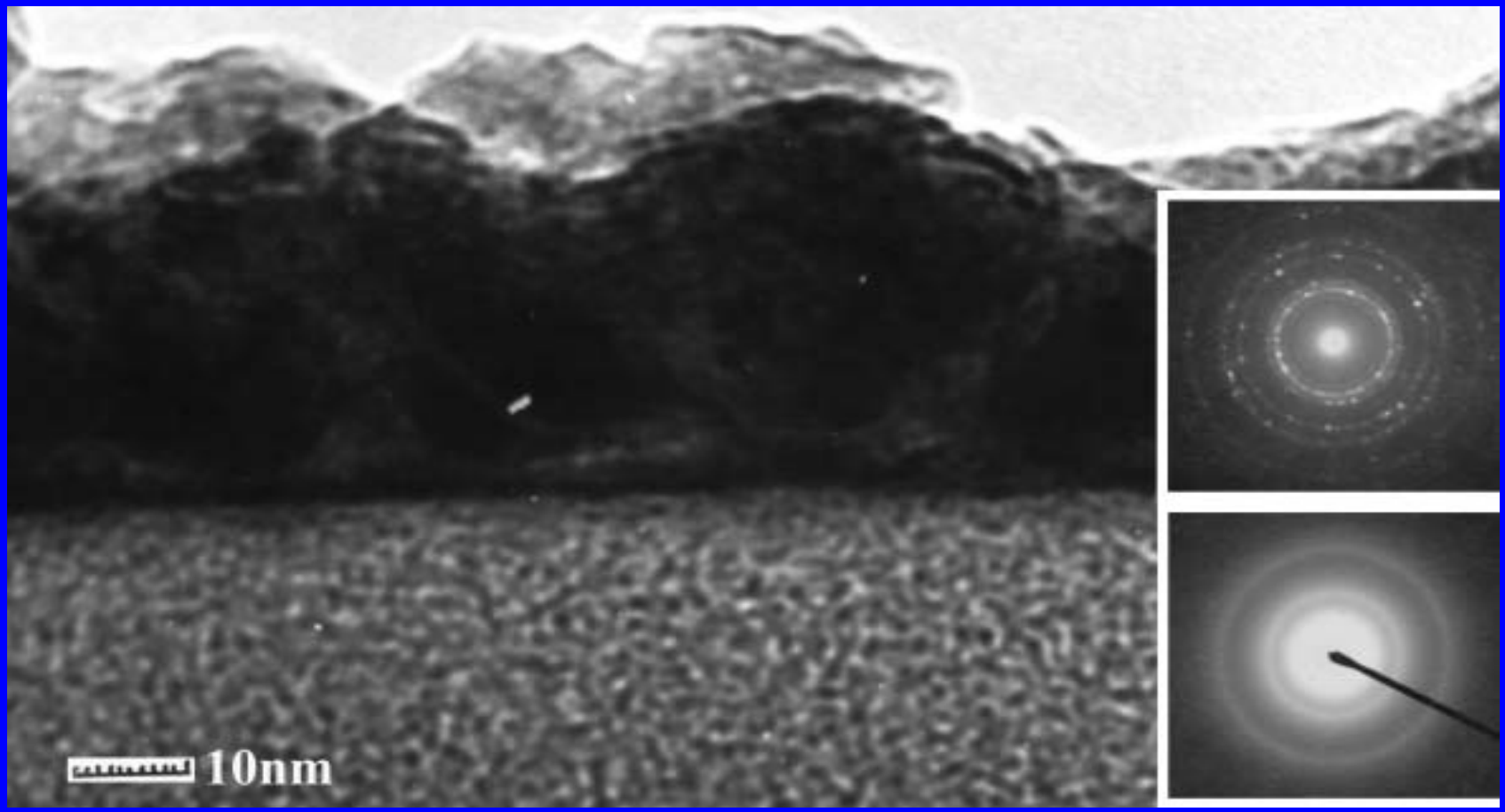

❑ 典型的球形硬碳SEM照片

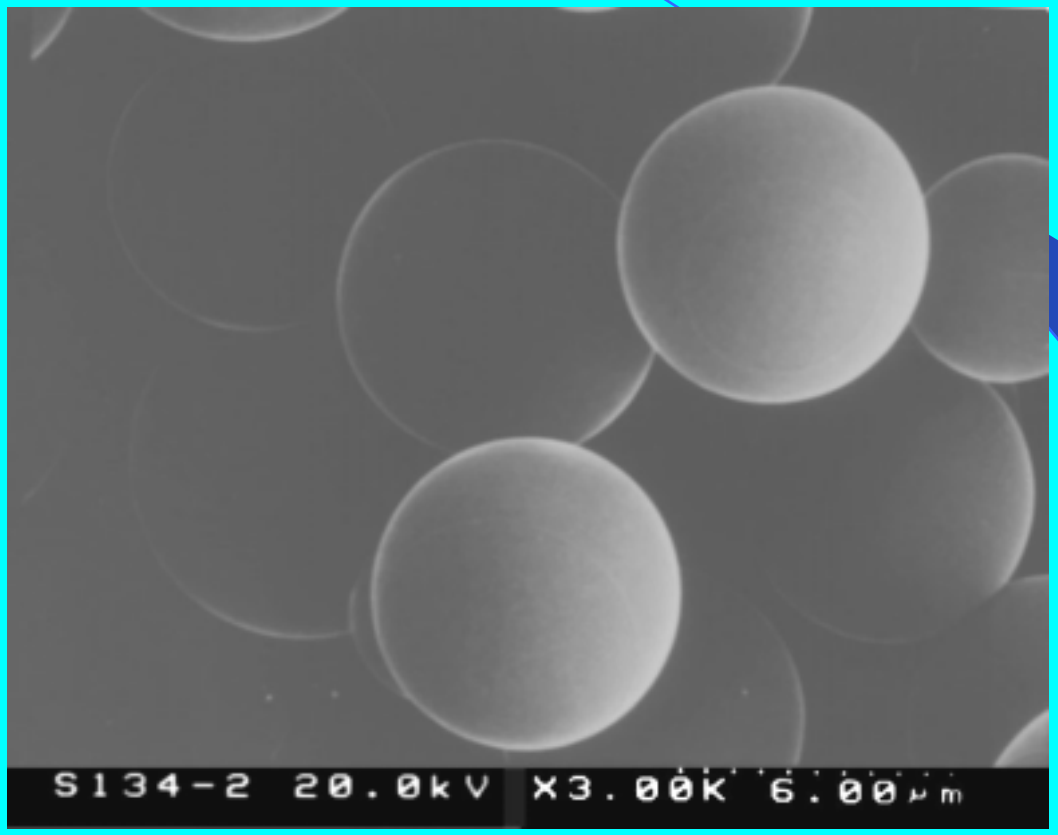

Perfect Spherical Morphology, Controllable Monodispersed Particle Size and Smooth Surface

HCS的高分辨透射电镜照片

- 典型的无定形碳材料
- 由单碳层堆积而成
- 分布着1 nm以下的微孔

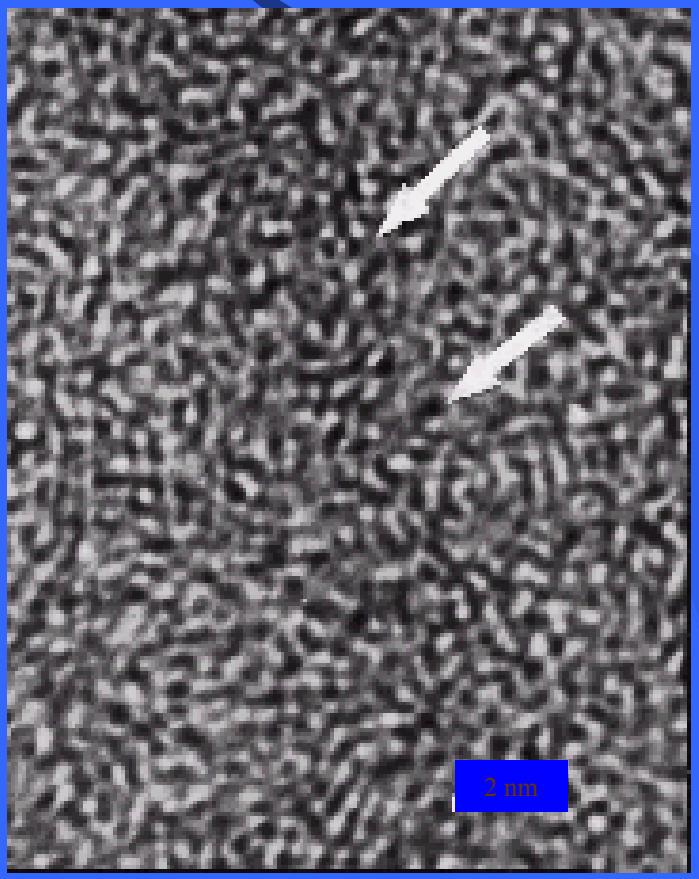

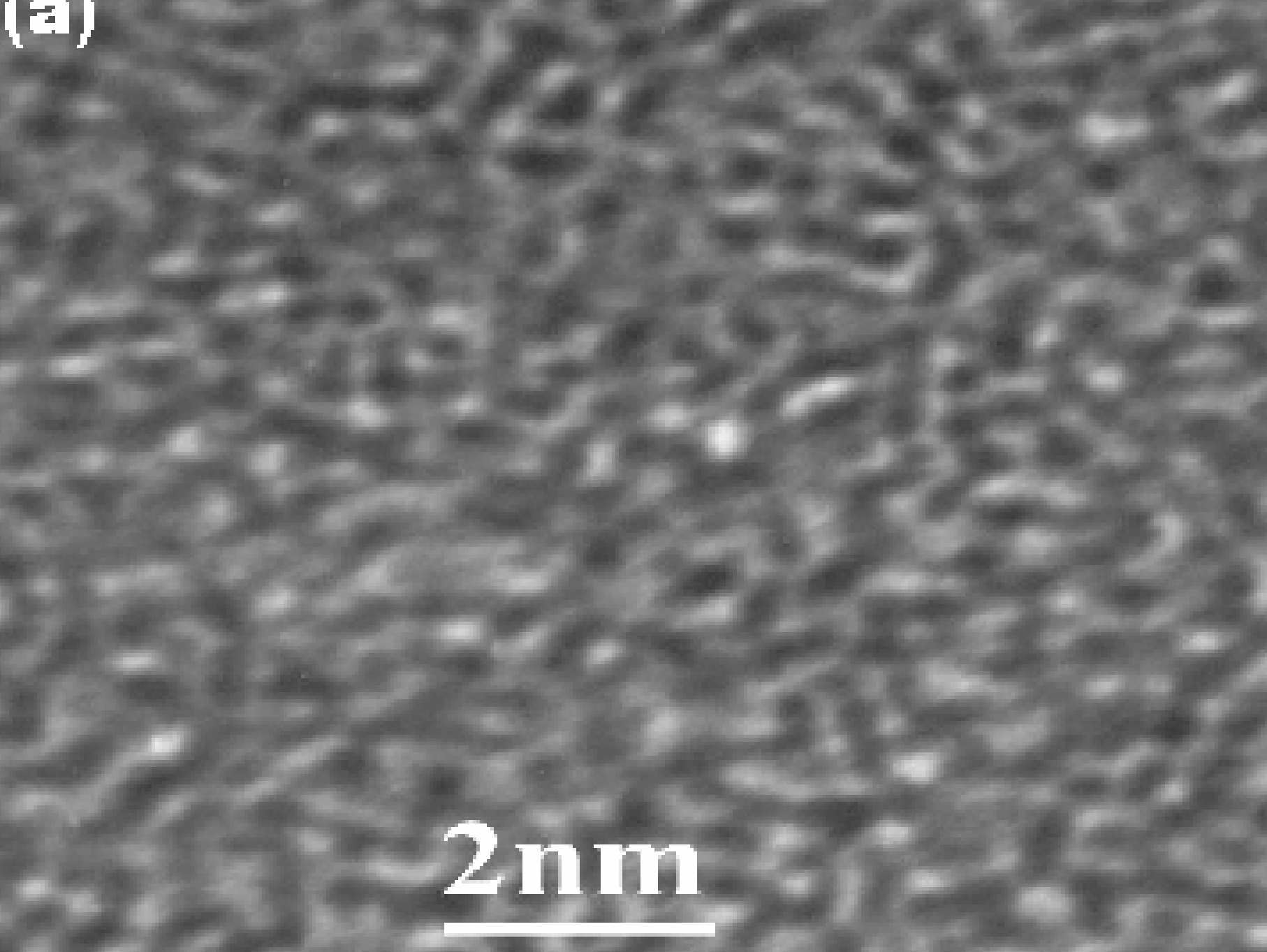
(a)
2nm

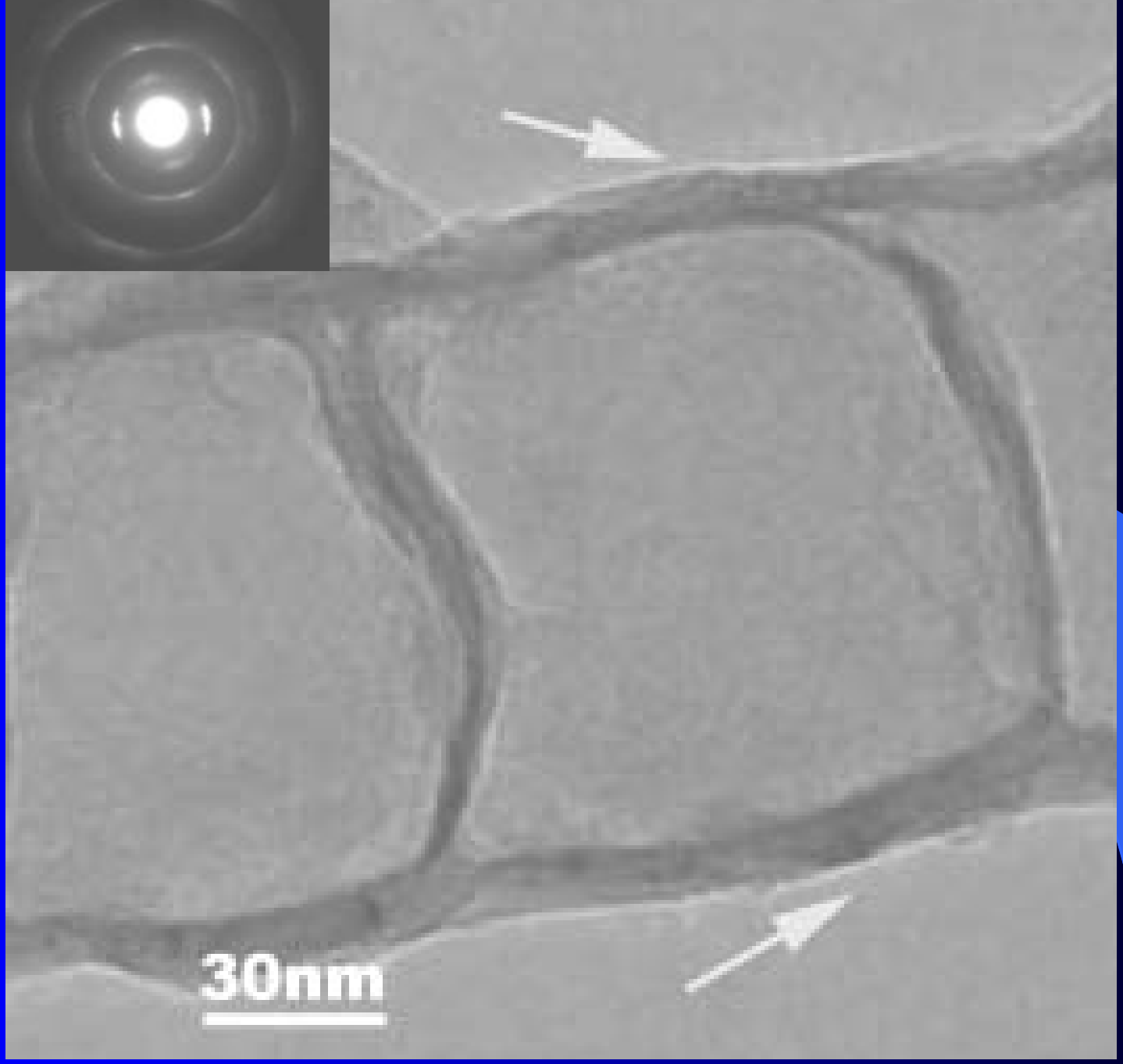
30nm

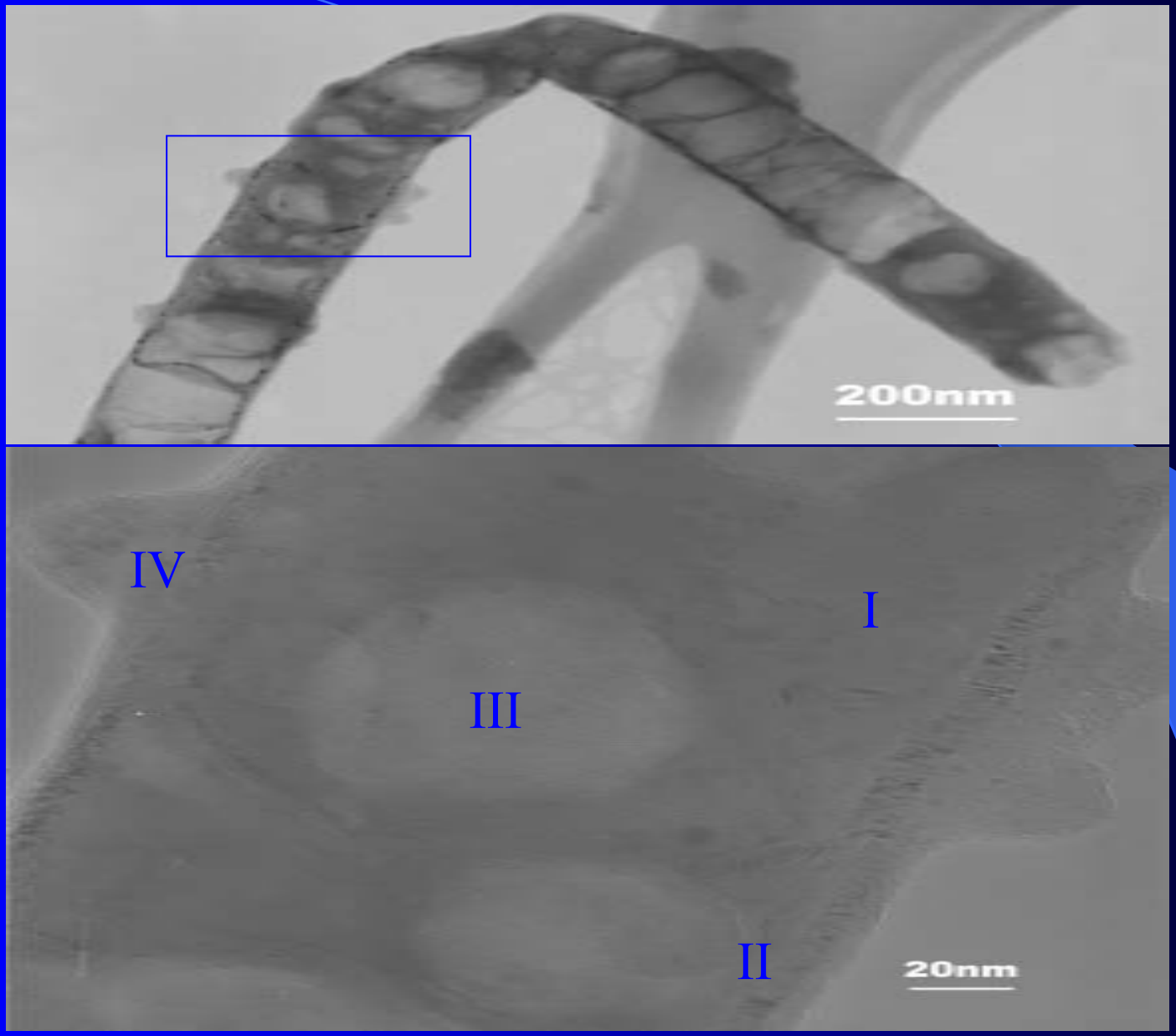
200nm
IV
I
III
II
20nm

III

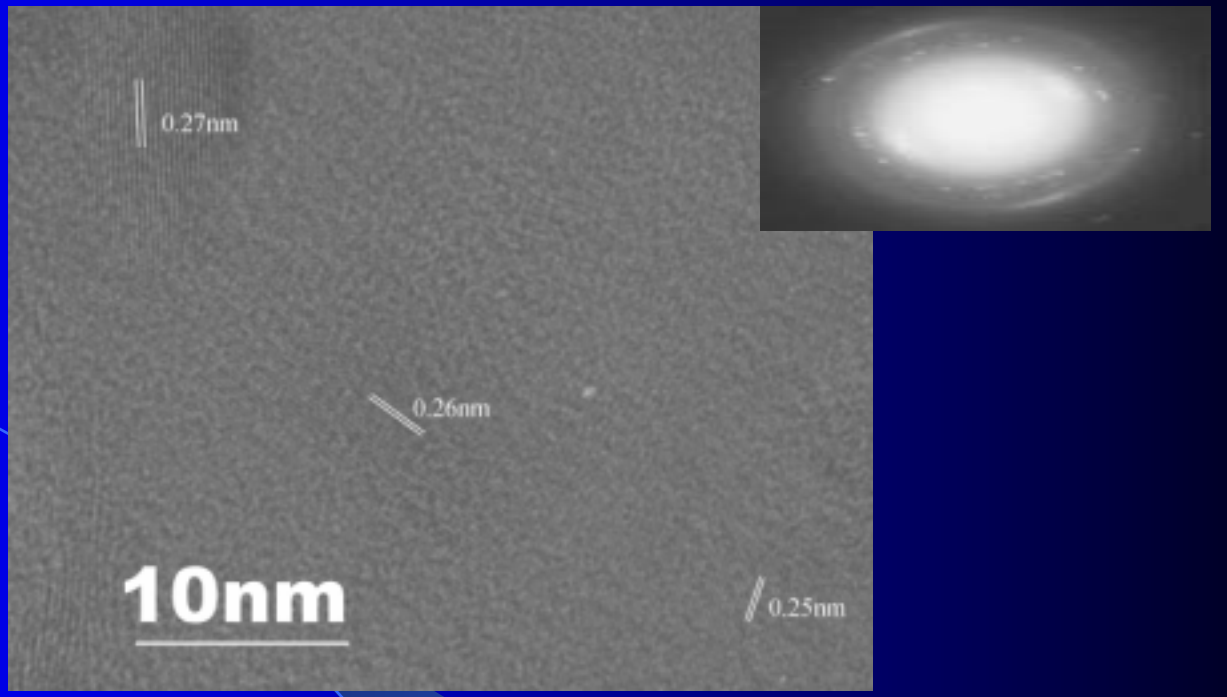

IV

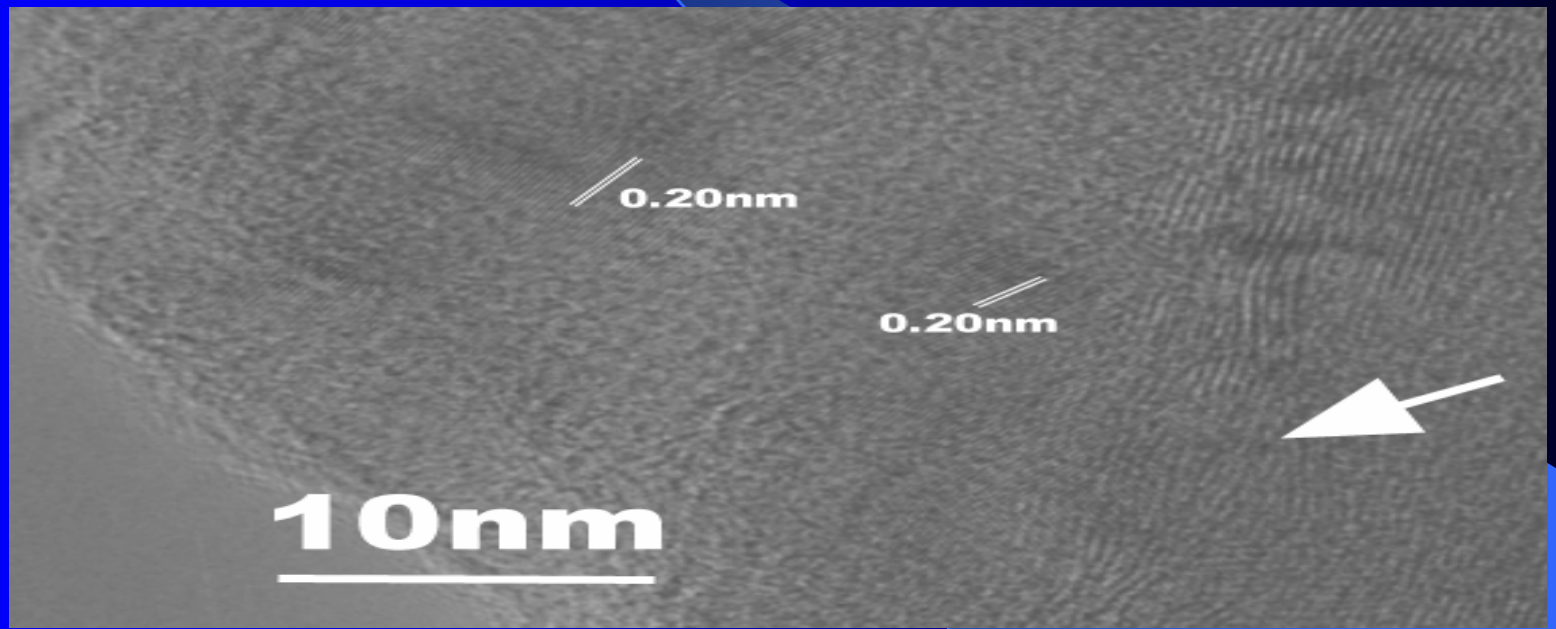

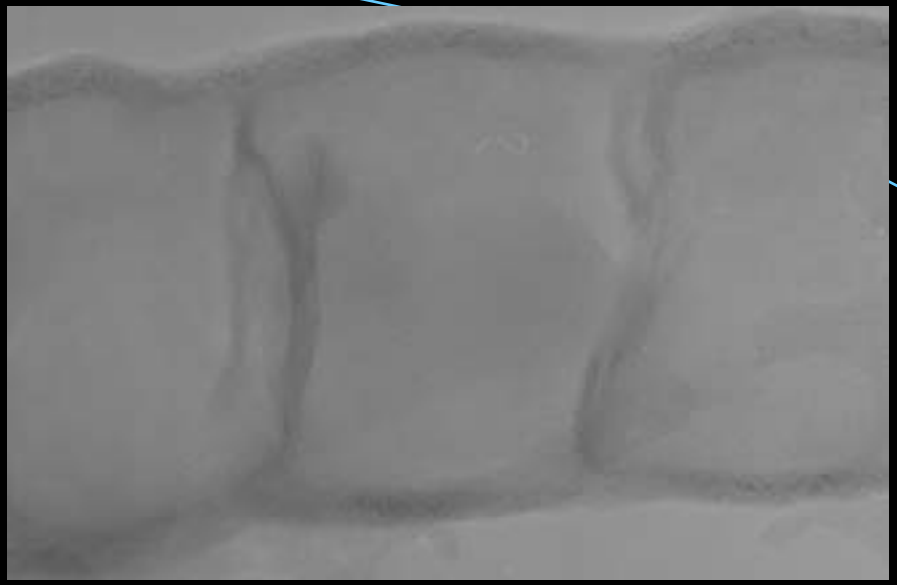

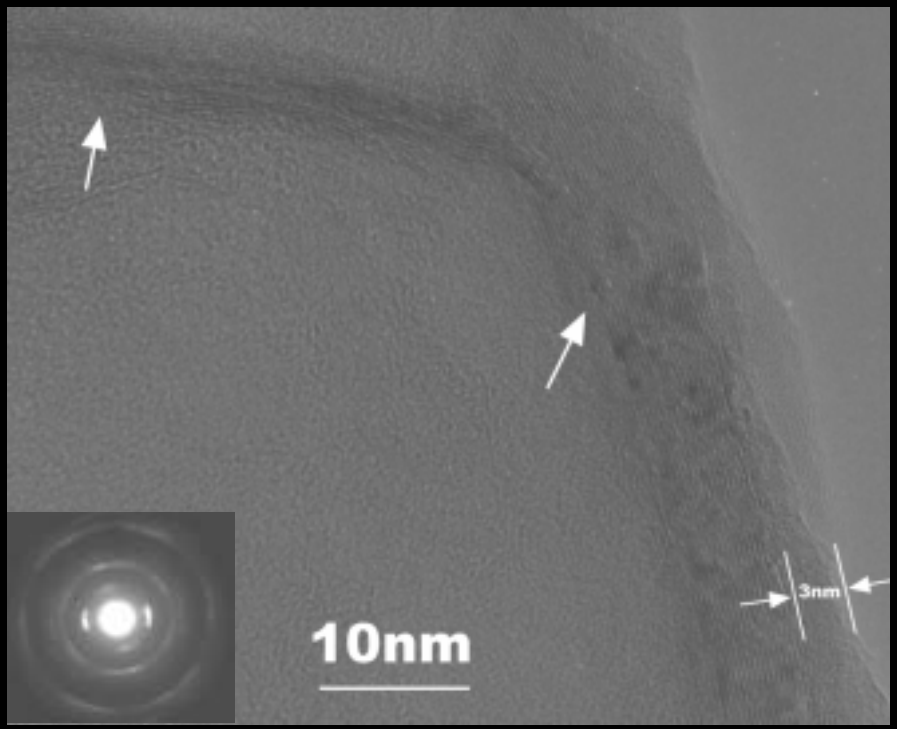

重要结论

在深嵌锂态观察到管内出现了大量新相的晶格条纹，在脱锂态这些条纹消失。根据条纹间距初步认为在管内壁形成了锂的高压相。这对多孔炭材料的嵌锂机理的研究有重要意义。

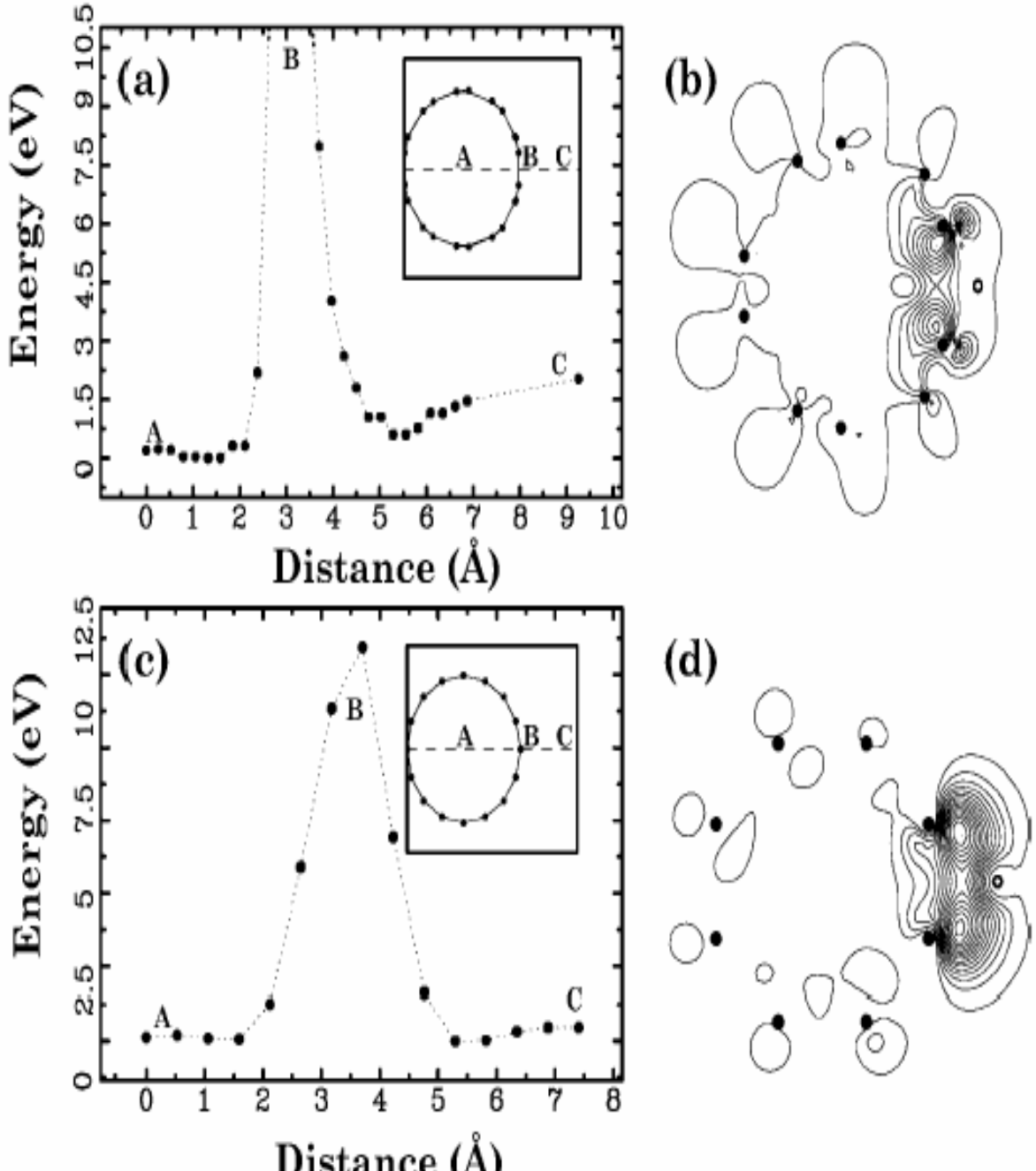

FIG. 1. Energetics of diffusion pathways for Li to move through a (a) $(5,5)$ metallic; and (c) $(8,0)$ semiconducting nanotube. Contour plots of the resulting charge difference distribution for a Li atom absorbed on $(5,5)$ and $(8,0)$ nanotubes are shown in (b) and (d), respectively. The positions of the C(Li) atoms are indicated by the filled (open) circles, respectively.

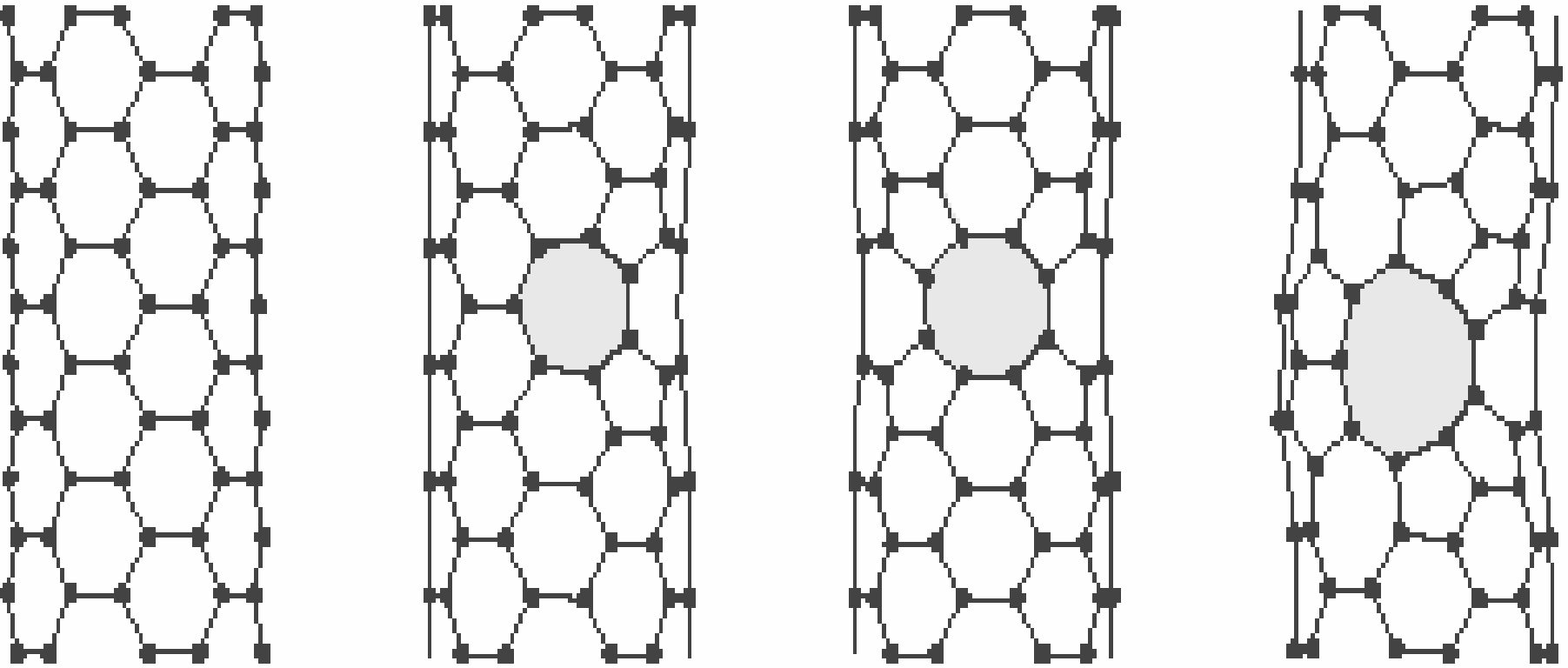

FIG. 2. Structure of the topological defects displaying differ-
ent n-membered rings. The diffusion barriers through these rings
and the corresponding formation energies are given in Table I.

TABLE I. Diffusion barrier ΔE and formation energy E_F for each of the topological defects shown in Fig. 2. The formation energy is measured with respect to the hexagon.

	ΔE (eV)	E_F (eV)
Hexagon	13.5	0.0
Heptagon	7.5	3.5
Octagon	3.0	6.2
Enneagon	0.5	9.5

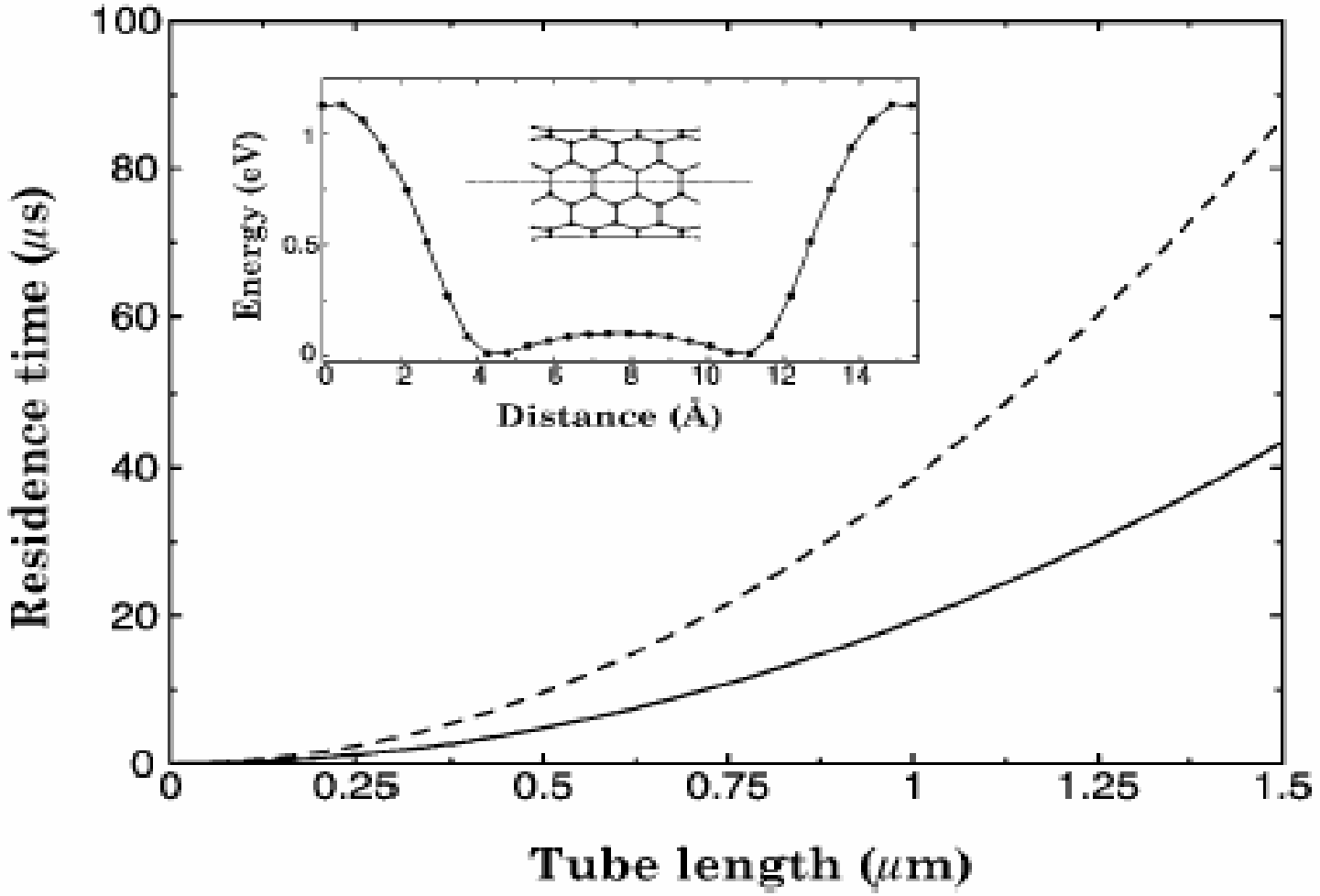

FIG. 3. Estimated residence time τ as a function of nanotube length L at $T = 300$ K for Li atoms in either the nanotube interior (solid line) or interstitial rope channel (dotted line). The inset shows the energetics of a typical diffusion path calculated for Li moving through an open nanotube.

New Li-reactivity mechanisms

➡ **Our group**: Poizot et al. Nature, 407 (6803), 496-499 (2000).

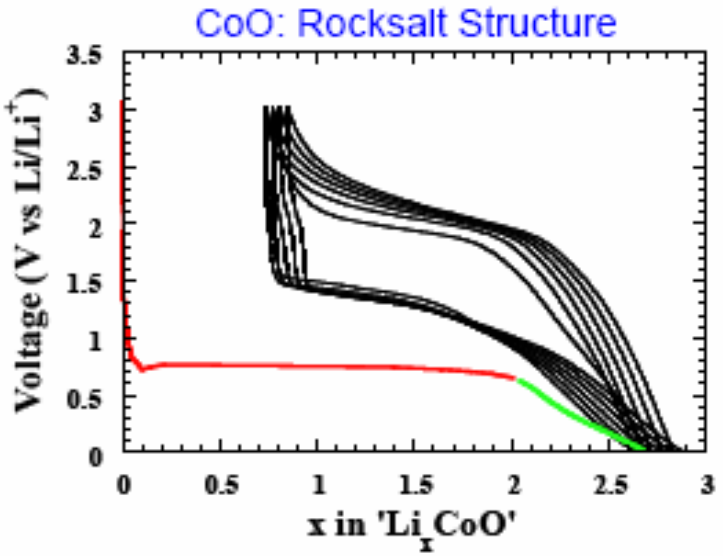

☞ No Interstitial voids for guest ions

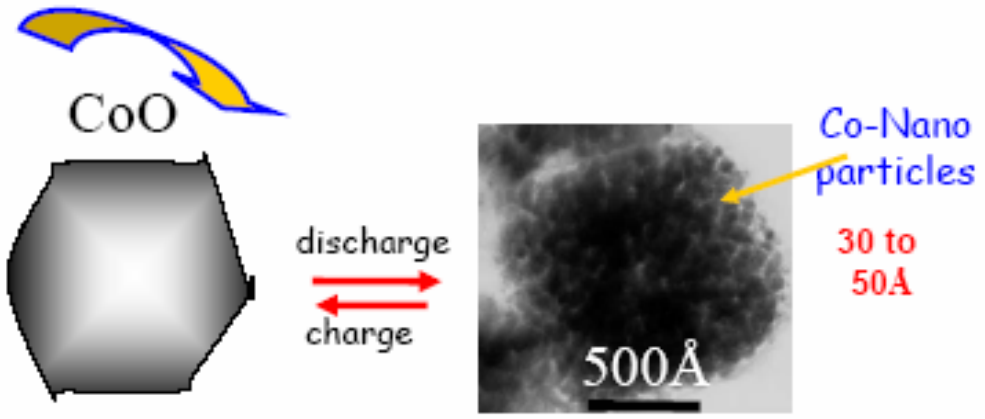

$$CoO + 2\,e^- + 2\,Li^+ \leftrightarrows Co^0 + Li_20$$

2 e⁻ per Co

M^{n+} to M^0 "Conversion reactions"

factor 3

Today Li-ion cells

$Li_xCoO_2 + 0.5Li^+ + 0.5e^- <=> LiCoO_2$

0.5-0.6 e⁻ per Co

MO_x/M° reactions of conversion : Not specific to CoO, but universal

Same behavior observed for :

- Sulfides, Fluorides, Chlorides, Phosphides and Nitrides

0.7 V ↓ 3.5 V

$$NiP_2 + 6\,e^- + 6\,Li^+ \leftrightarrows Ni + 2\,Li_3P$$
$$CoO + 2\,e^- + 2\,Li^+ \leftrightarrows Co^0 + Li_2O$$
$$CoCl_2 + 2\,e^- + 2\,Li^+ \leftrightarrows Co^0 + 2\,LiCl$$
$$CoF_3 + 3\,e^- + 3\,Li^+ \leftrightarrows Co^0 + 3\,LiF$$
$$RuO_2 + 4e^- + 4Li^+ \leftrightarrows Ru^0 + 2\,Li_2O$$

2 to 6 e^-

Today Li-ion cells

$Li_xCoO_2 + 0.5Li^+ + 0.5e^- \Leftrightarrow LiCoO_2$

0.5-0.6 e^- per Co

Staggering capacity gains (factor 4 to 5)

Poizot et al. Nature, 407 (6803), 496-499 (2000).

Microstructure evolution of RuO_2 after Li-insertion and extractio

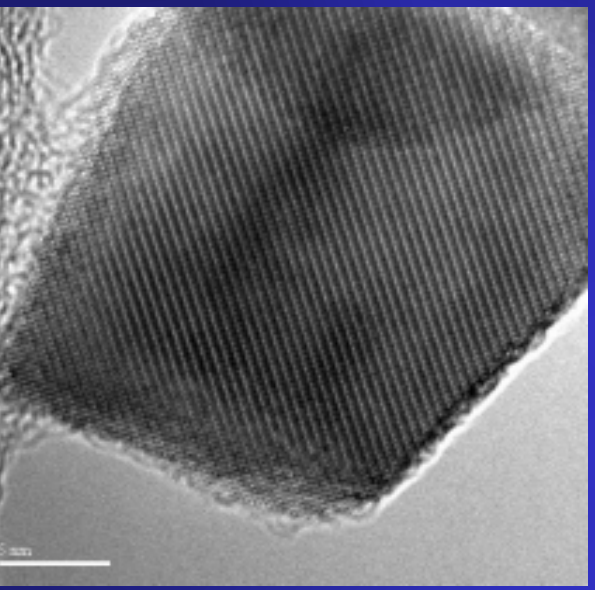

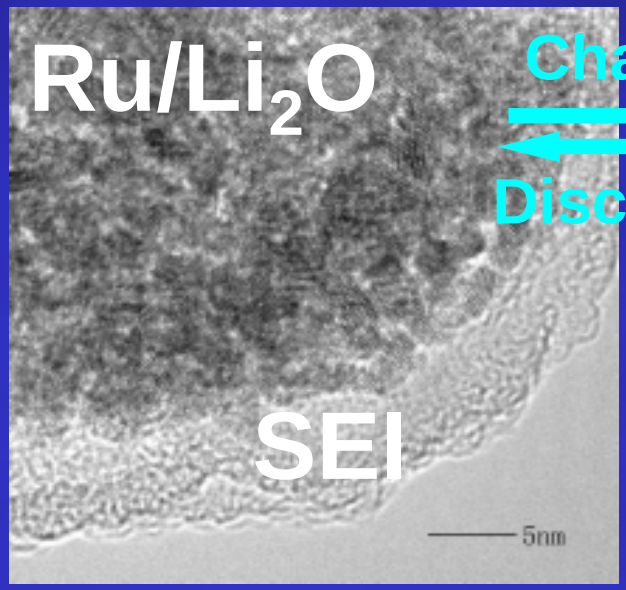

Charge

Discharge

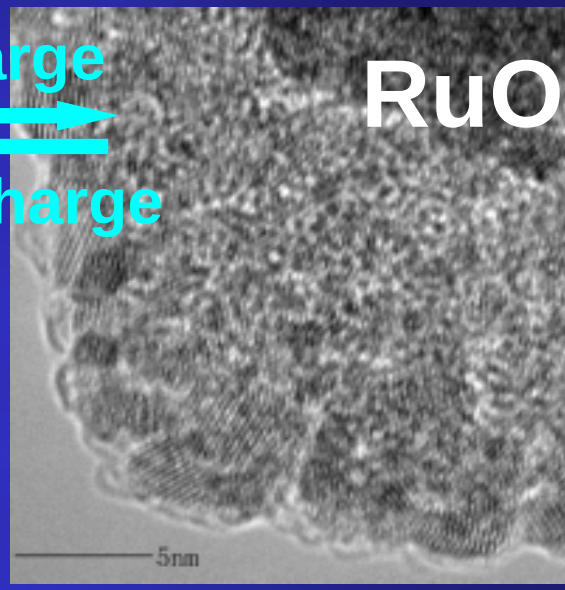

$\mu m\text{-}RuO_2 + 4\ Li \rightarrow 2\ Li_2O/Ru\ (2\text{-}5\ nm) \rightleftharpoons nm\text{-}RuO_2$

P. Balaya, H. Li, J. Maier, *Adv.Func. Mater.*, 13, 621(200

Microstructure evolution of TiF_3 caused by Li insertion/extraction

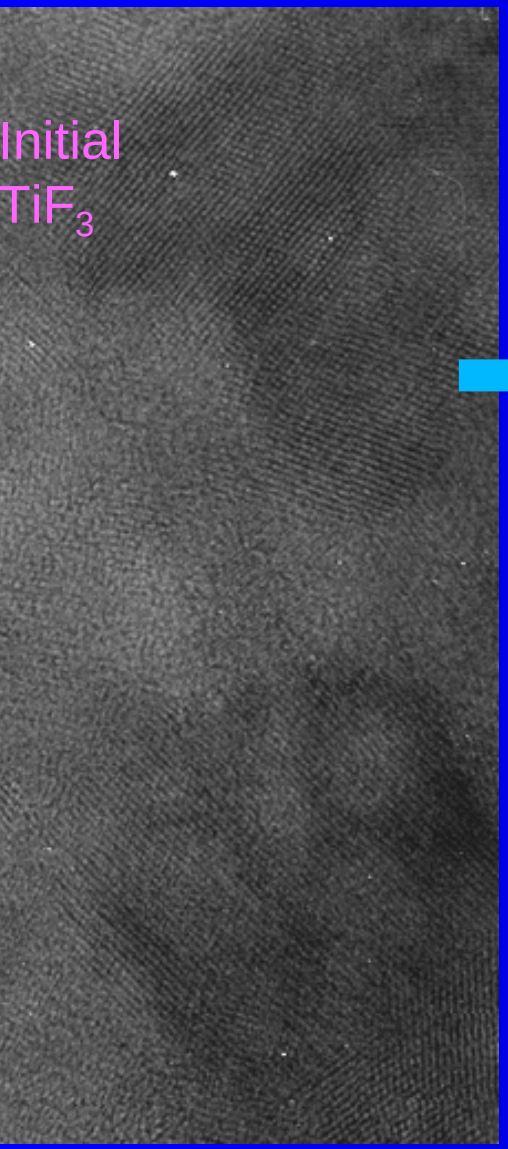

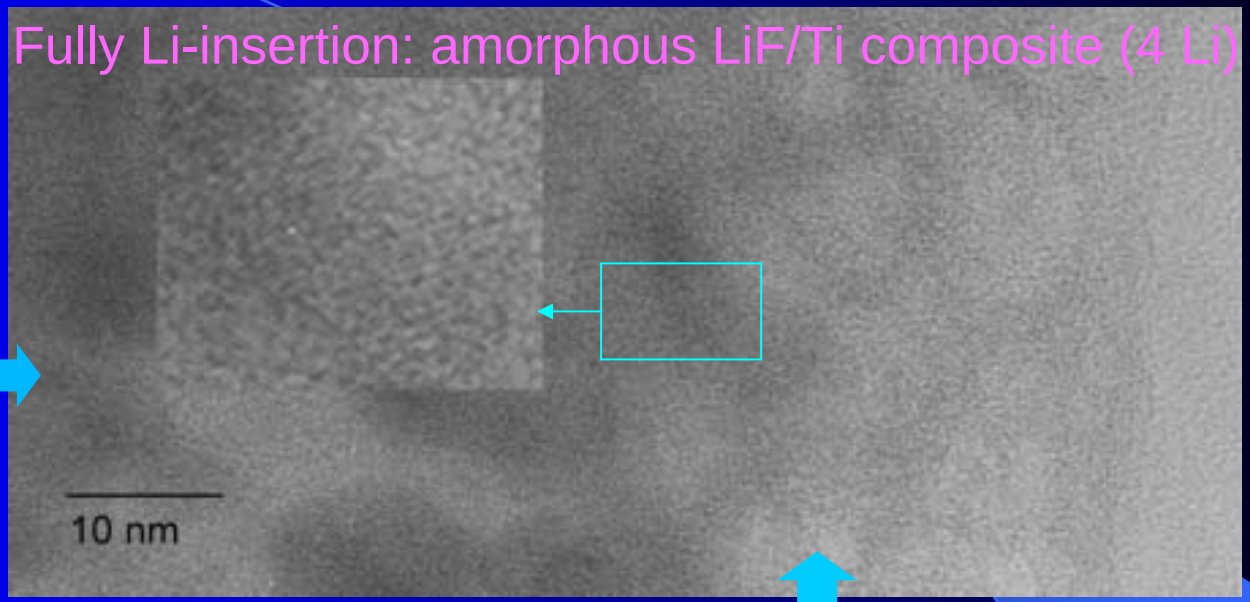

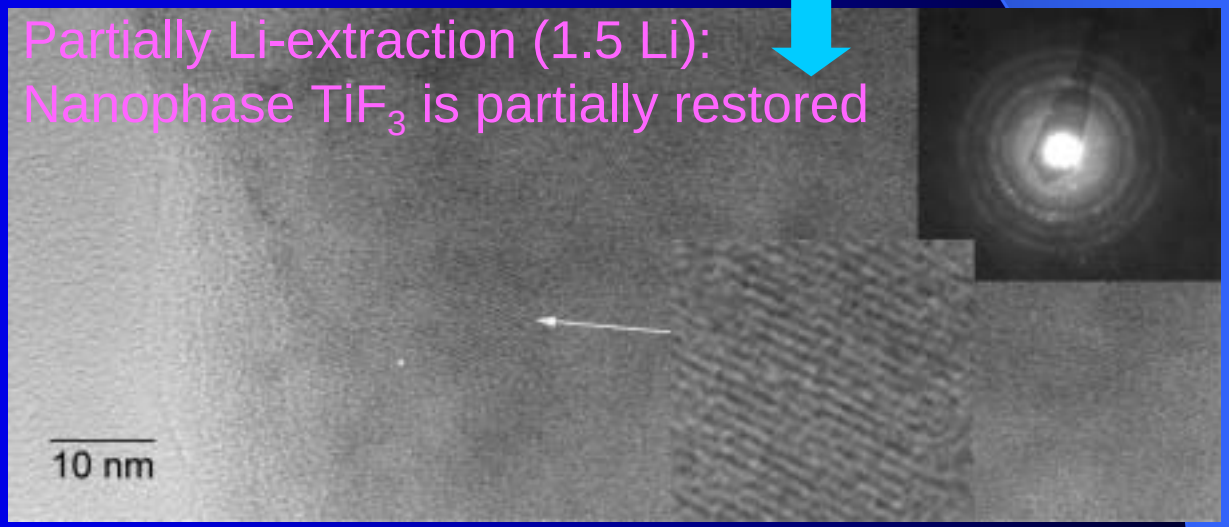

$Li + TiF_3 \leftrightarrow LiF + Ti$ (amorphous)

H. Li et al. *Adv. Mater.* 15, 736(2003)

A scheme for back-reaction LiX + M → MX ?

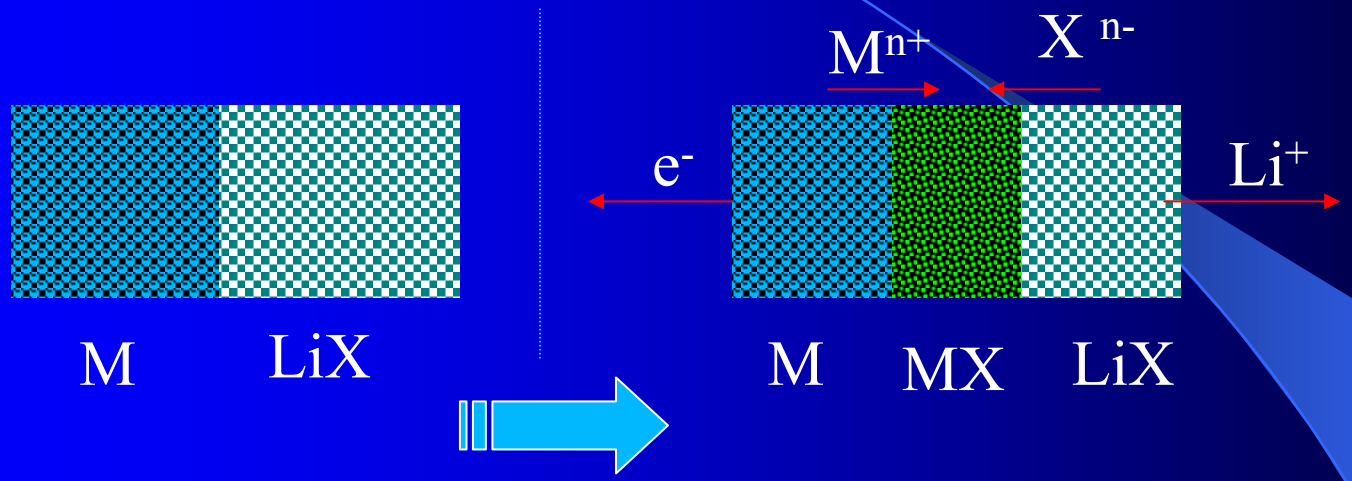

diffusion of either M^{n+} or X^{n-} across the interphase : MX

LiX and M dispersed at atomic or nanoscale is key point
or occurrence of back-reaction in view of kinetics.
Experimental data confirm this!

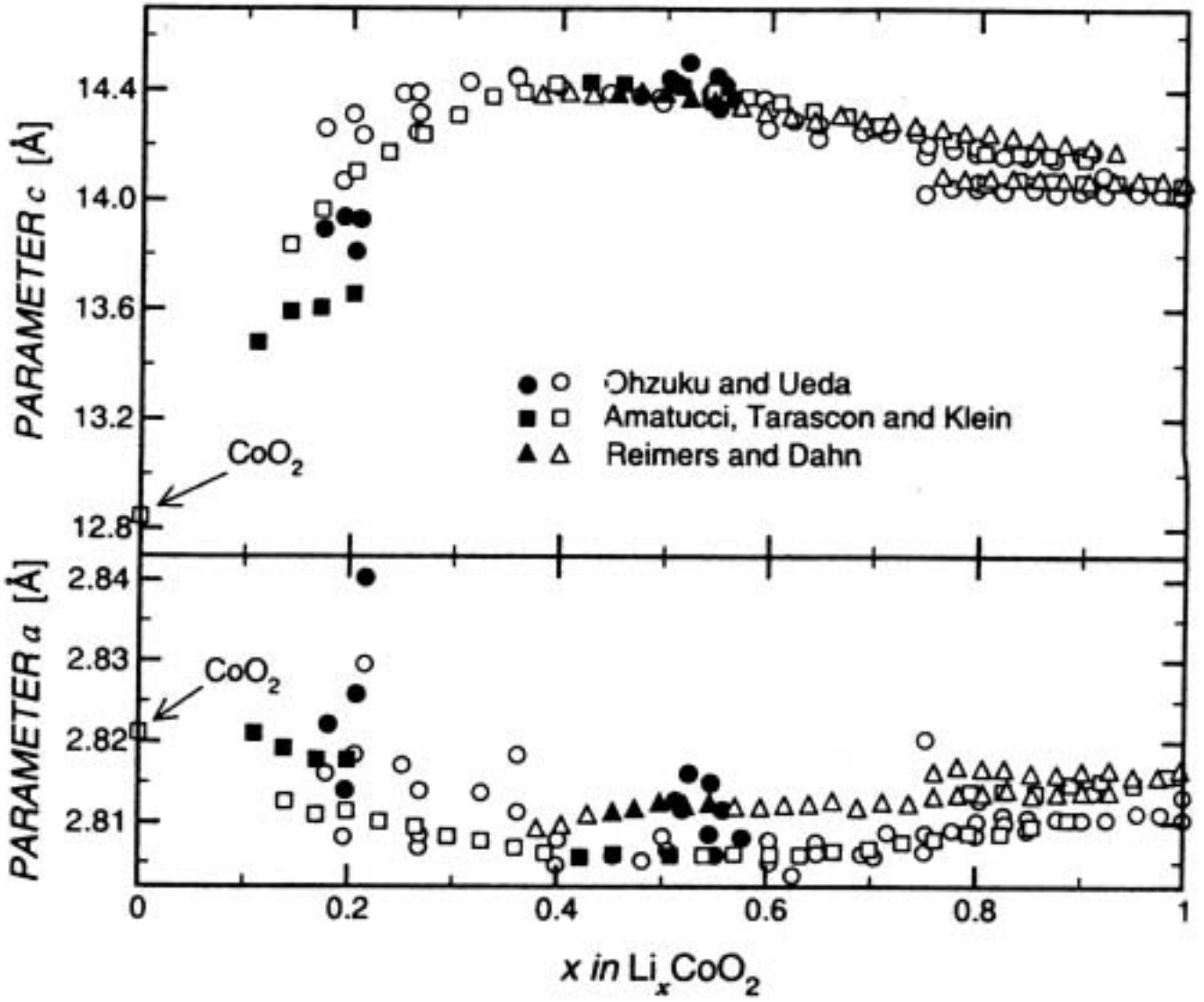

Fig. 9. Lattice parameters of hexagonal unit cell of Li_xCoO_2 [18,22,23] (filled symbols represent monoclinic phases parameters converted to hexagonal parameters).

The specific capacity of commercial $LiCoO_2$ fades rapidly when overcharged (to a. 4.3V; b. 4.5V and c. 4.7V, respectively).

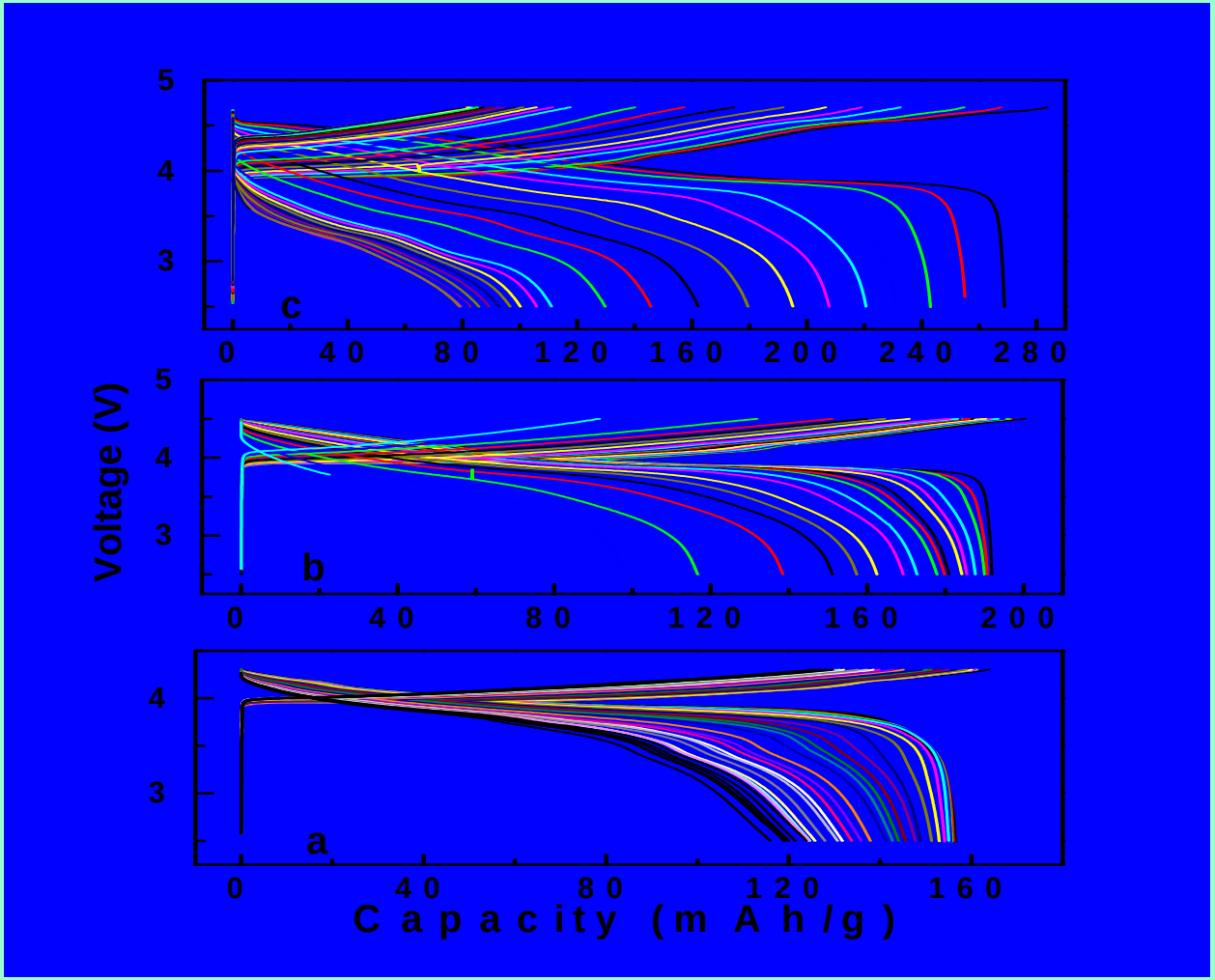

Comparison of morphology of $LiCoO_2$ before (a) and after surface coating with MgO (b), SnO_2 (c) and Al_2O_3 (d).

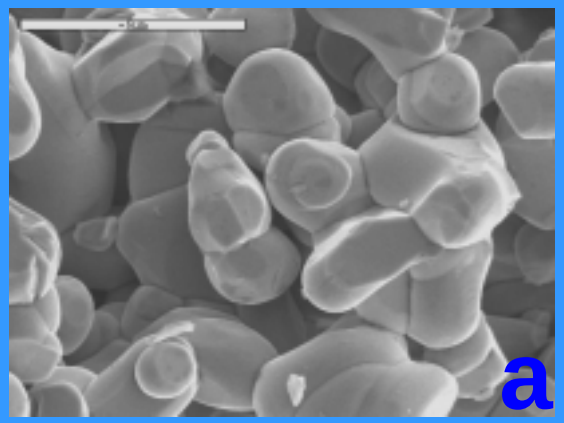

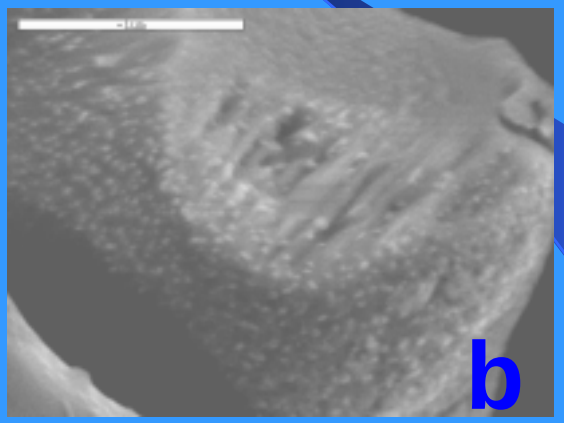

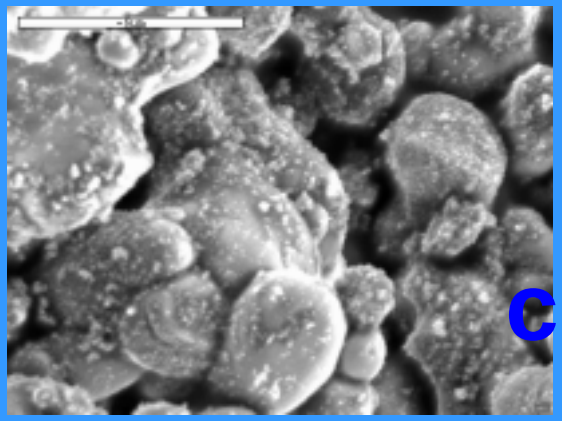

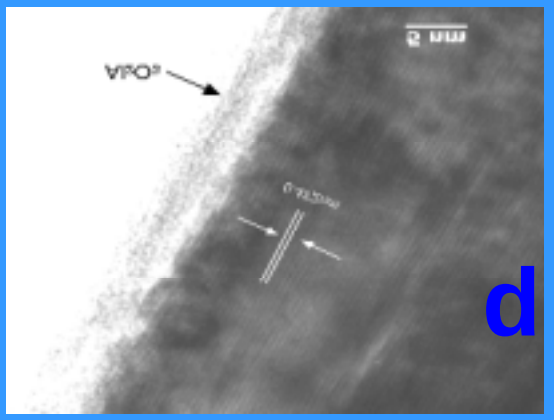

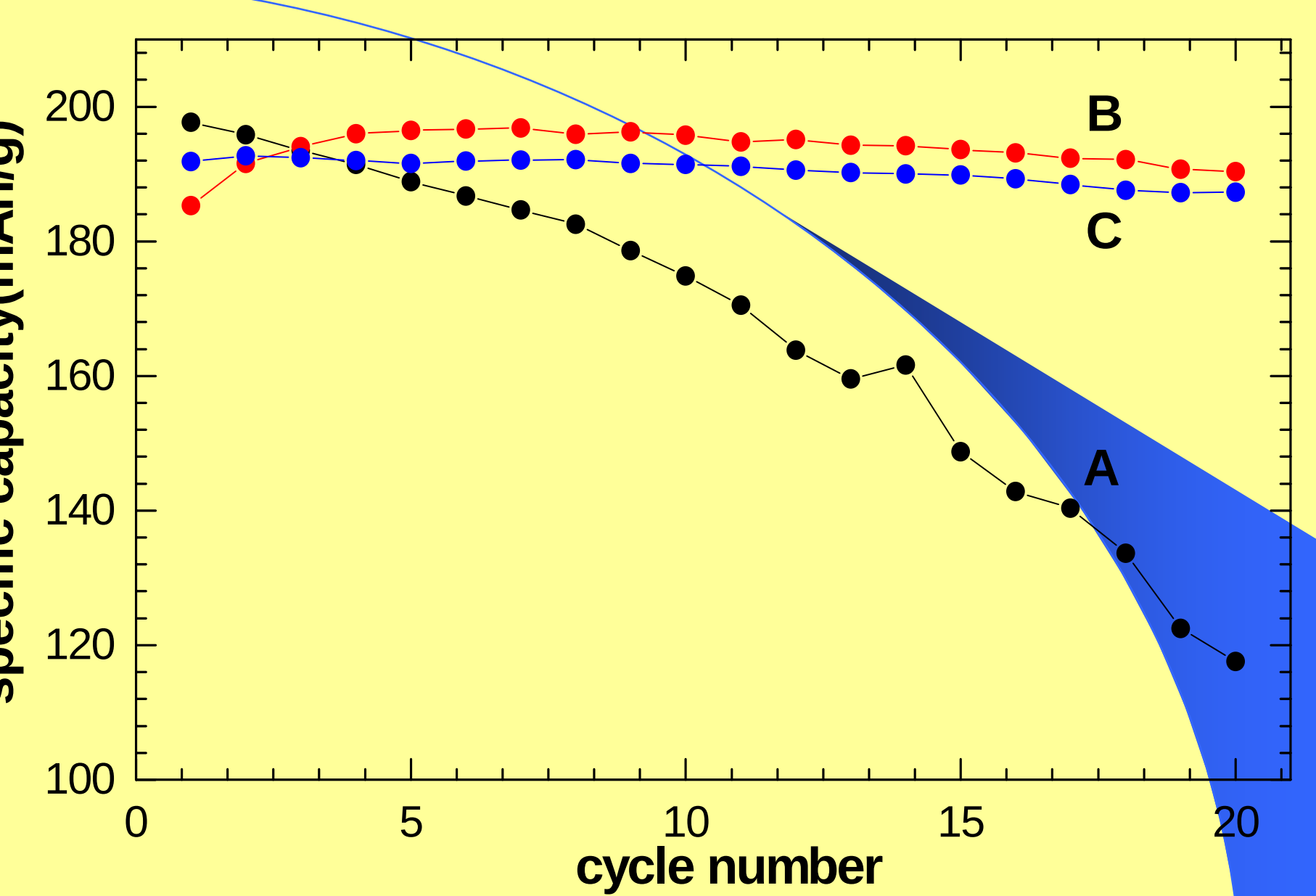

.pristine LiCoO2; b,c coated with nano-Al2O3 and MgO respectively

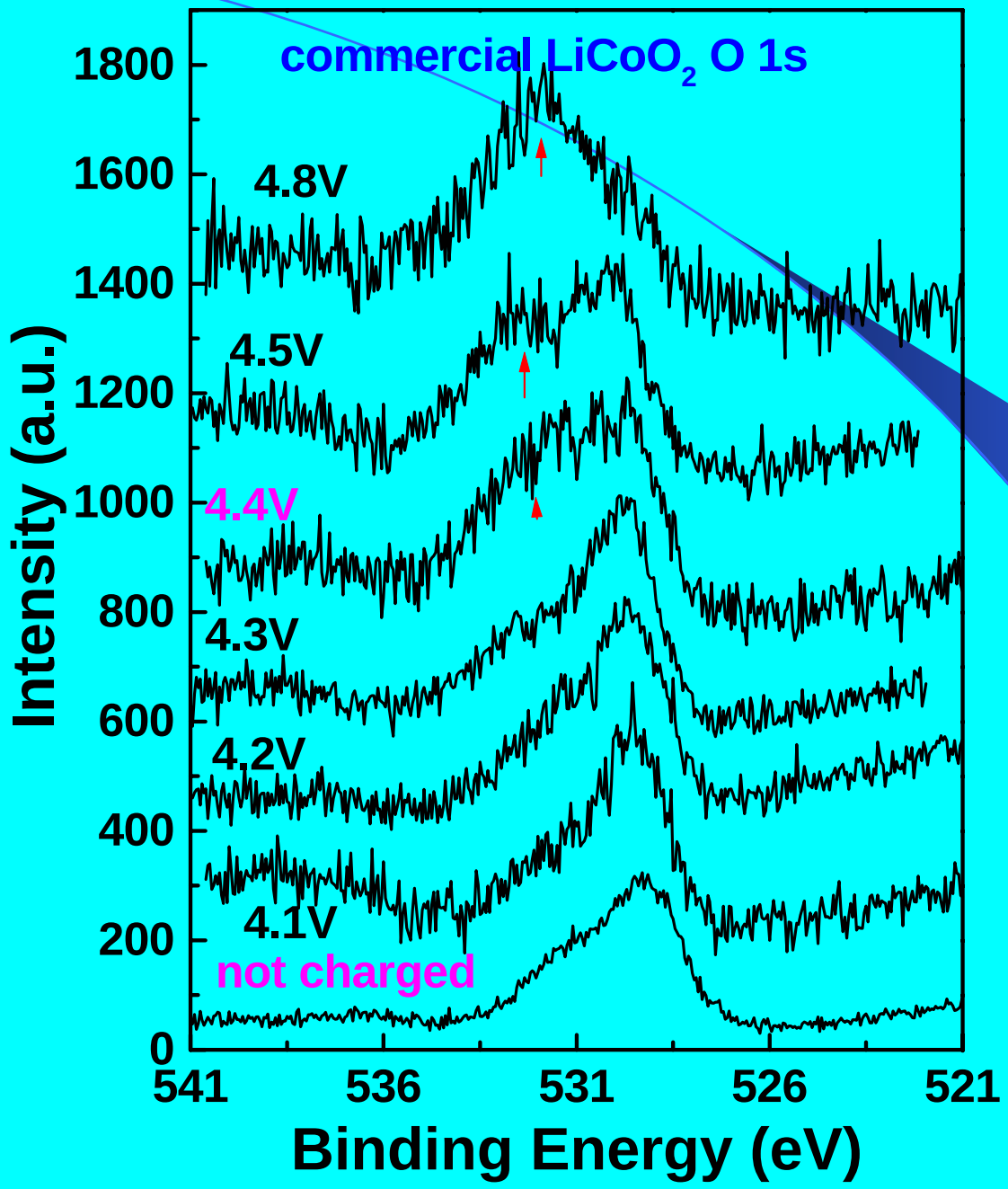
commercial LiCoO2 O 1s
1800
1600
1400
1200
1000
800
600
400
200
0
Intensity (a.u.)
4.8V
4.5V
4.4V
4.3V
4.2V
4.1V
not charged
541
536
531
526
521
Binding Energy (eV)

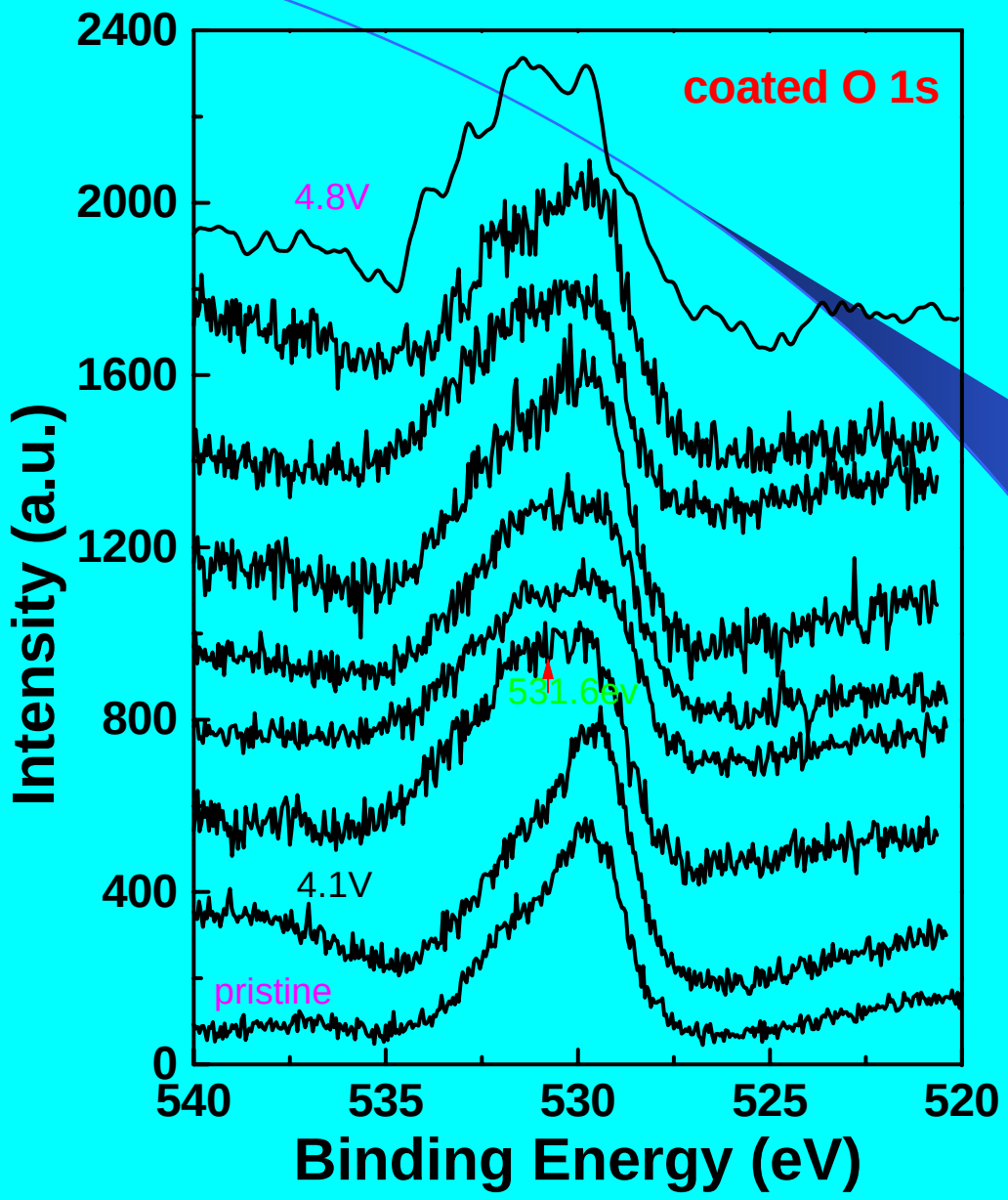
coated O 1s
4.8V
531.66eV
4.1V
pristine
Intensity (a.u.)
Binding Energy (eV)
2400
2000
1600
1200
800
400
0
540
535
530
525
520

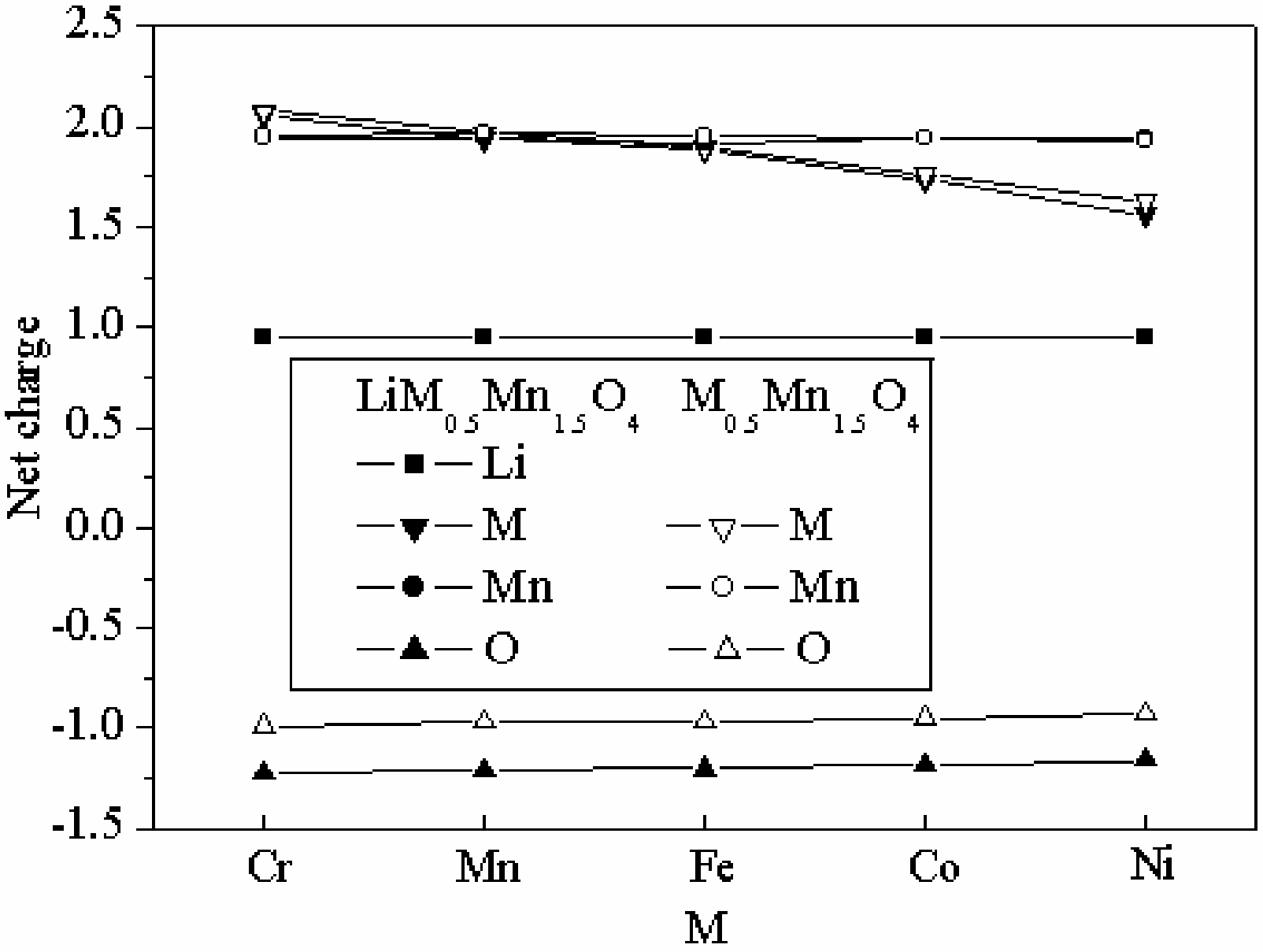
2.5
2.0
1.5
1.0
0.5
0.0
-0.5
-1.0
-1.5
Net charge
LiM0.5Mn1.5O4
M0.5Mn1.5O4
Li
M
M
Mn
Mn
O
O
Cr
Mn
Fe
Co
Ni
M

- 电荷转移和净电荷（电离度）

一方面，对给定的M, 可以通过分析$LiM_{0.5}Mn_{1.5}O_4$和 $M_{0.5}Mn_{1.5}O_4$ 来理解脱嵌的影响。

不难发现，由脱嵌引起的电荷转移主要来自O, 而不是Mn和M.

另一方面，可以通过比较$LiM_{0.5}Mn_{1.5}O_4$中M上的净电荷，来分析不同掺杂的影响。我们可以看出，Mn上的净电荷基本不受M的影响(这与以前的结论一致).

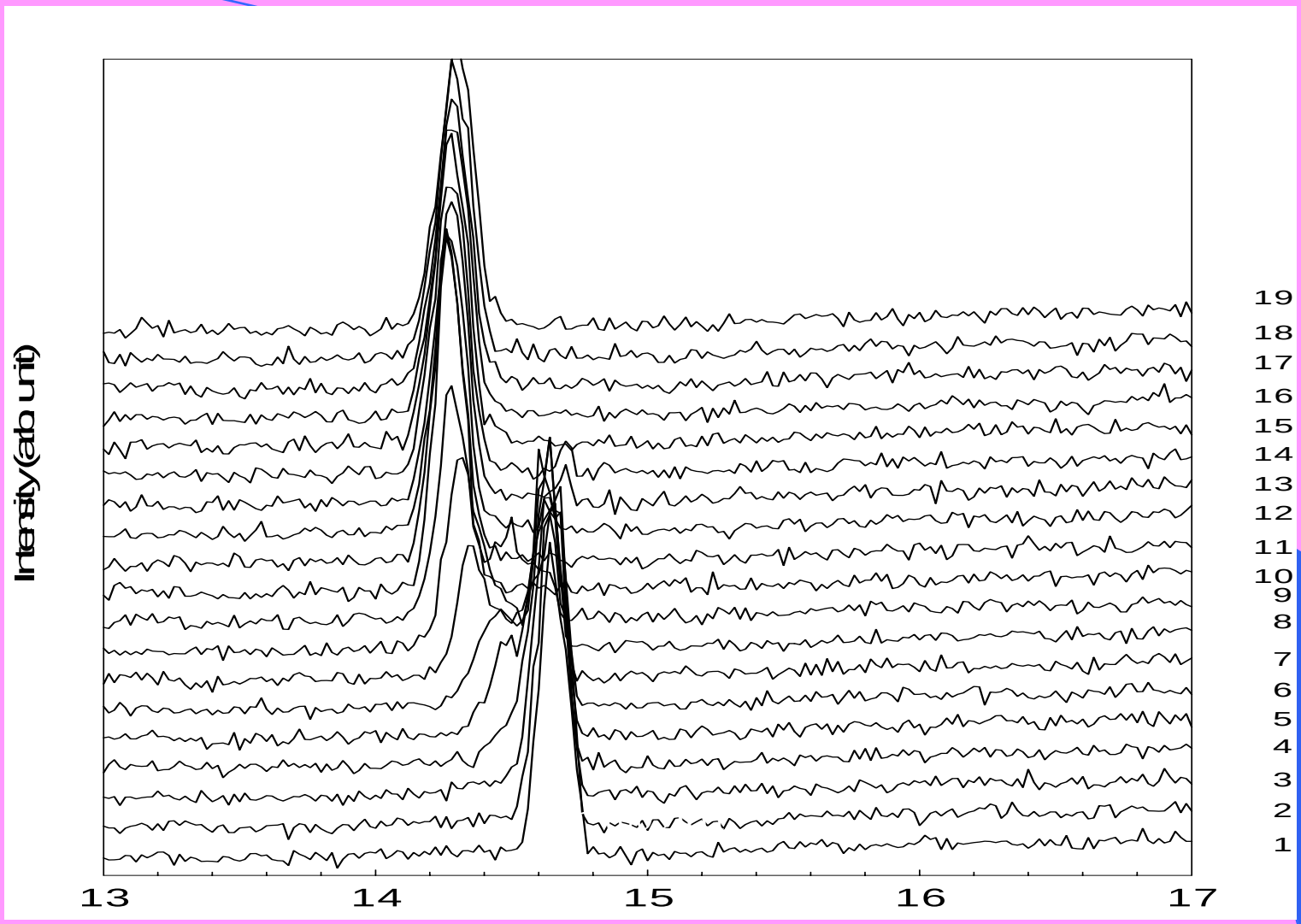
Intensity(arb unit)
13
14
15
16
17
19
18
17
16
15
14
13
12
11
10
9
8
7
6
5
4
3
2
1

2θ

Figure 6.a

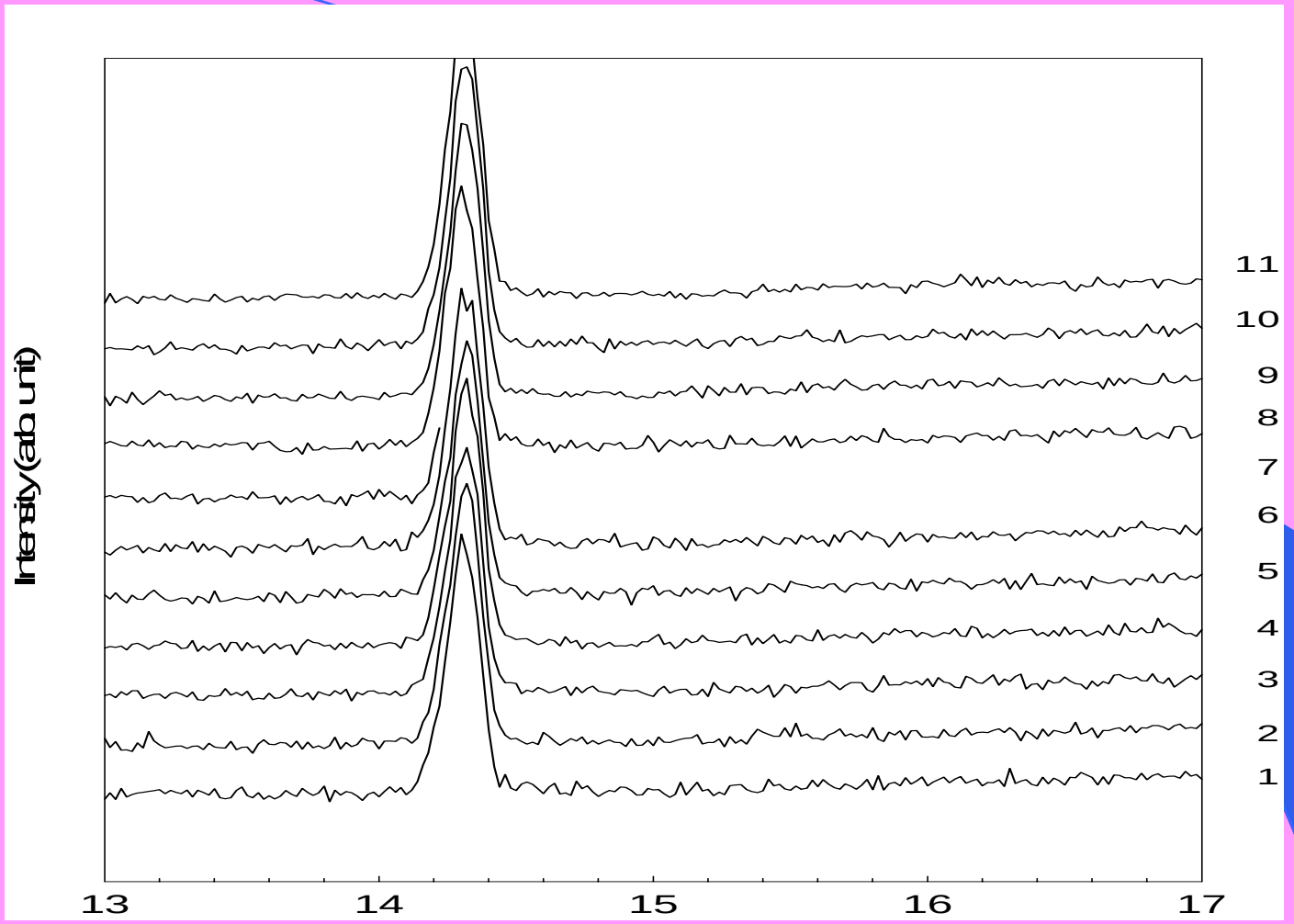

Figure 6.b

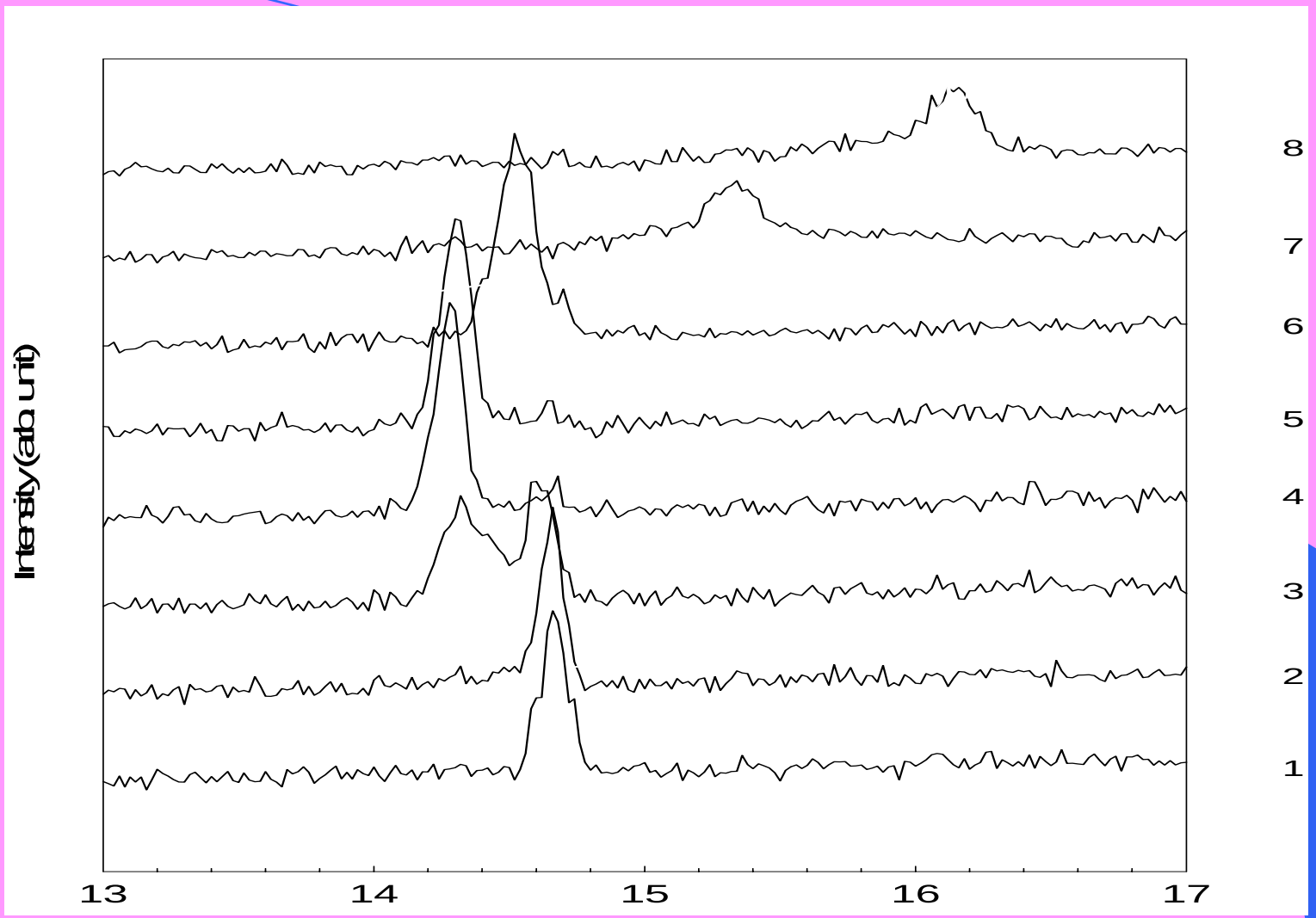

Figure 7.a

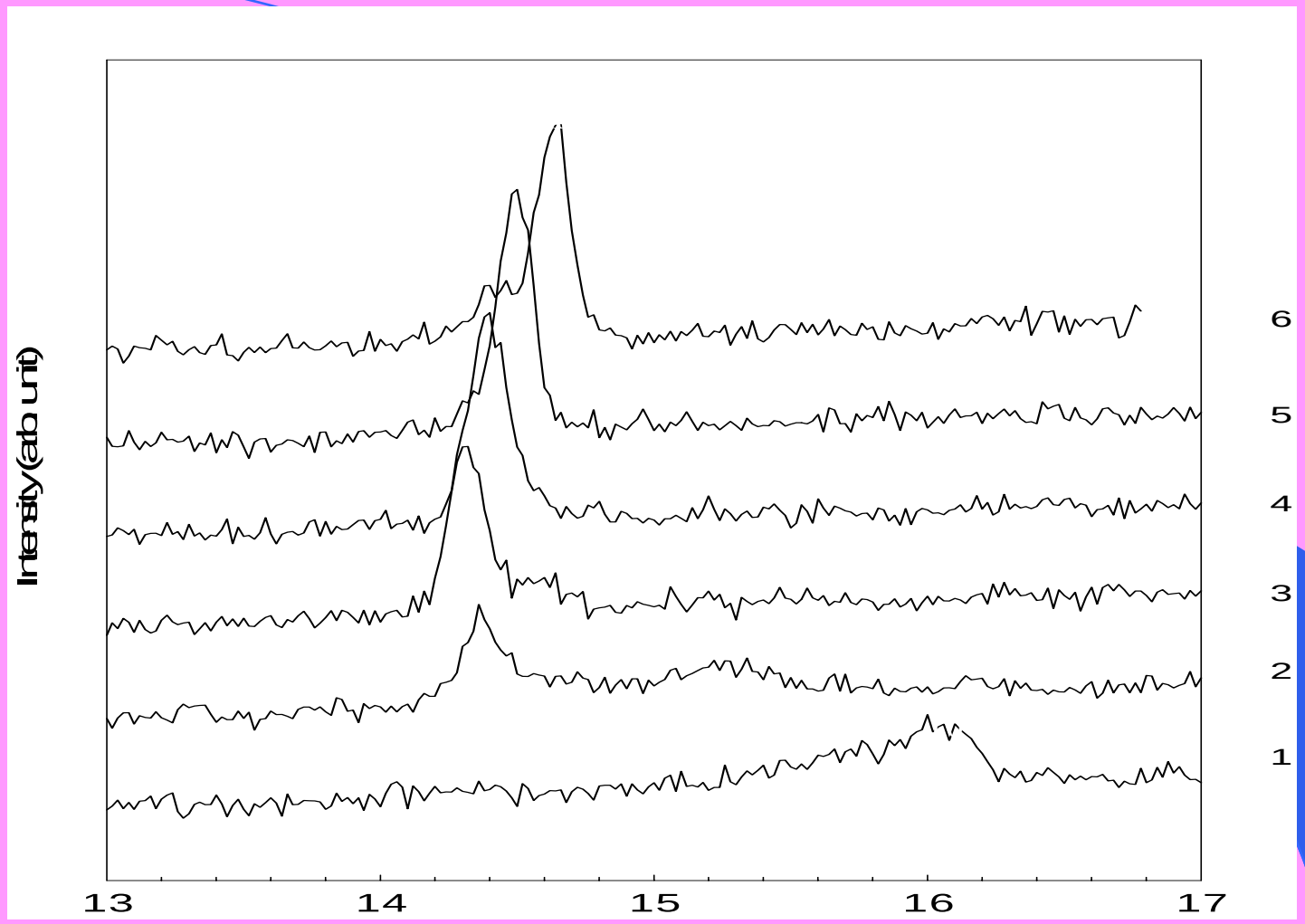

2θ

Figure 7.b

② From oxides to Polyanionic structures $LiFePO_4$

Why ?

O^{2-} ⟶ $(PO_4)^{3-}$ ⇨ *Benefits of inductive effect*

Fe — + ionic — O — PO_3

Adjust the Fe^{+2}/Fe^{+3} redox potential by playing with # polyanions

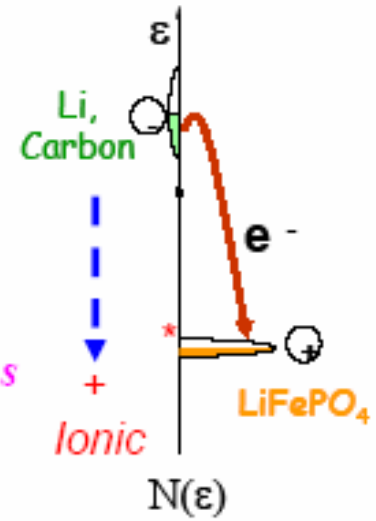

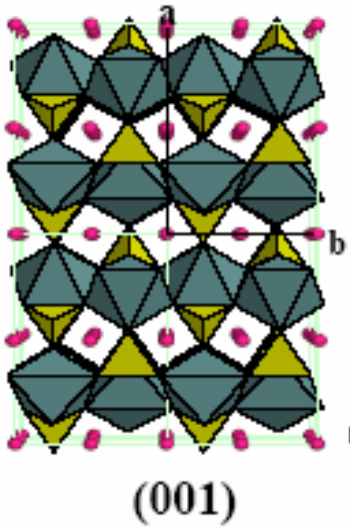

Olivine $LiFePO_4$

$LiFePO_4$ (Fe^{2+}) ⟷ $Li_{0.4}FePO_4$ (Fe^{3+})

3.5 V vs Li^+/Li ;

170mAh/g

Very poor electronic conductivity (Insulator)

A. K. Padhi, K. S. Nanjundaswamy, C. Masquelier, S. Okada and J.B. Goodenough, *J. Electrochem. Soc.* 144(5), 1609-1613 (1997)

Slow electronic conductivity: How to bypass this handicap ?

$$D_{chem} = \frac{\sigma_{electron}\sigma_{ion}}{\sigma_{electron} + \sigma_{ion}}$$

Percolation

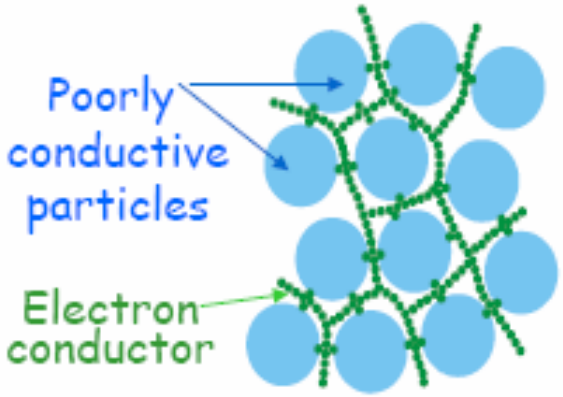

Ravet et al., ECS Meeting, Hawaï, 1999

Particles are connected, but the quality of contact may vary

Scrosati et al. IMLB XII, Nara 2004

Particle Coating

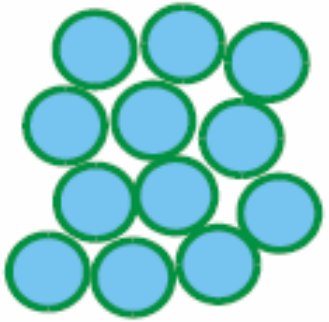

IMPORTANT:

Coating must be permeable for ions

Nano-architectured electrode

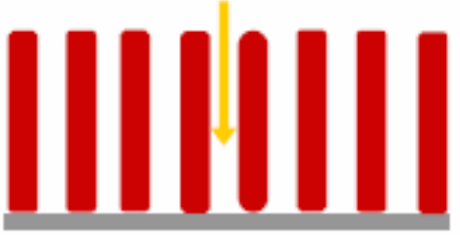

. Good electronic conductivity

. Direct electrolyte path

$LiFePO_4$的能带和态密度图

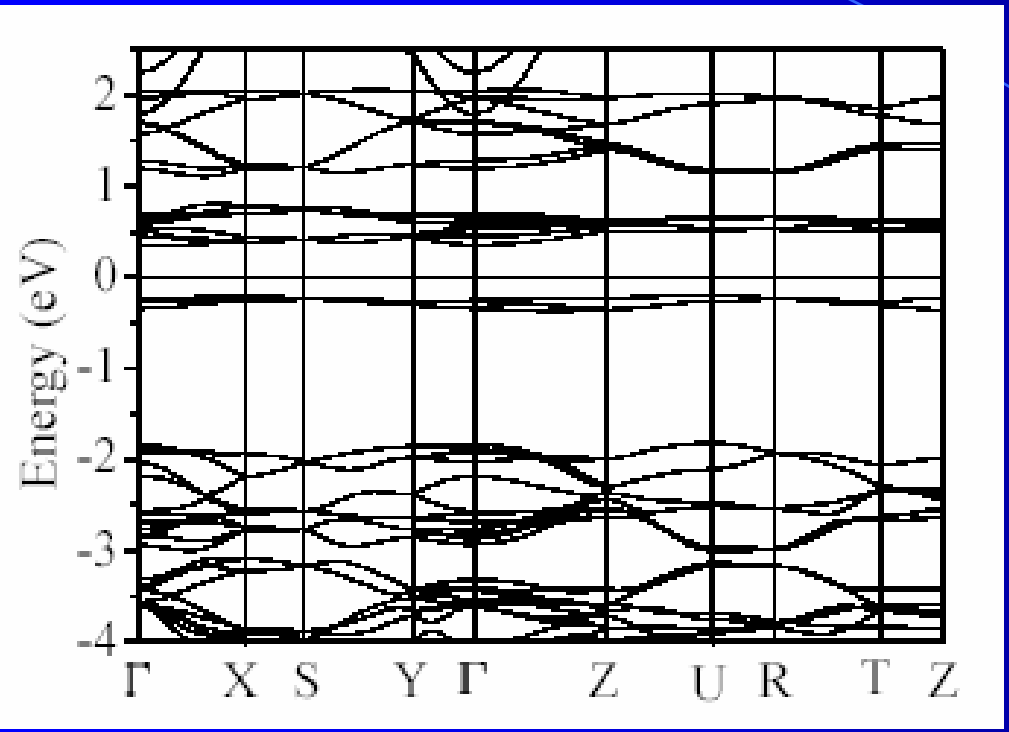

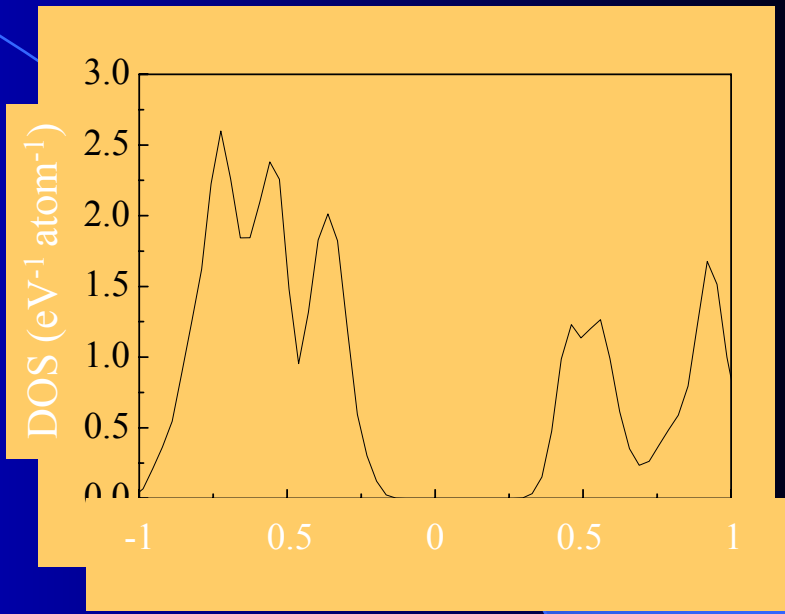

纯的$LiFePO_4$是一种典型的半导体，其理论上的带隙为0.53eV. 费米能级附近的窄带是Fe 的3d 部分. Fe 的非成键t_{2g} 态和反成键e_g 态分别位于-1 ~ -0.11eV 和0.28 ~ 1.5eV 的能量范围。

对$LiFePO_4$和$Li_{1-3/32}Cr_{1/32}FePO_4$的比较

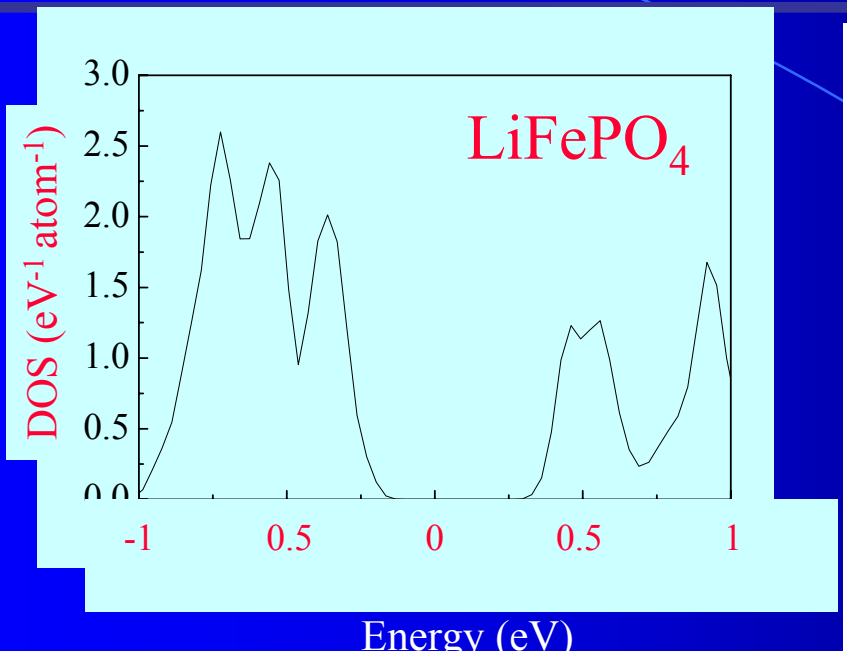

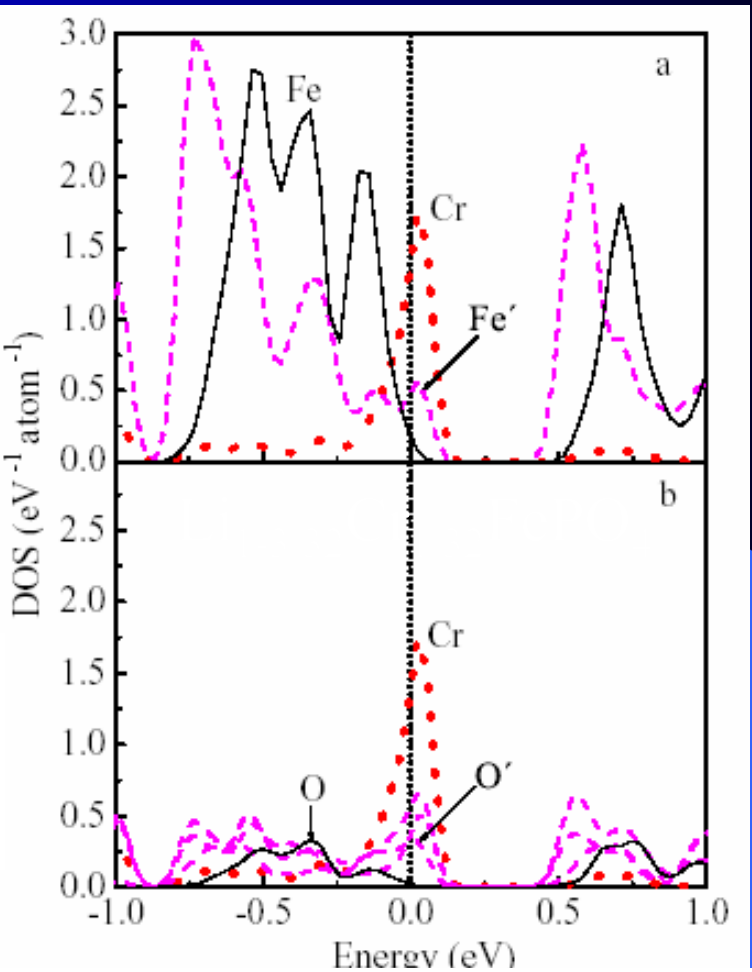

☹ 与纯的$LiFePO_4$相比，$Li_{1-3/32}Cr_{1/32}FePO_4$的费米能级位于价带顶偏下的地方，以至于在价带顶产生了空穴.

☹ 在$LiFePO_4$中,费米能级附近没有出现电子态.而在$Li_{1-3/32}Cr_{1/32}FePO_4$中,费米能级附近的电子态主要来自Cr 的3d, 同时也包含了Cr-3d 和邻近的O-2p、Fe-3d的杂化部分。我们认为正是这些电子态的出现才导致了电子电导率的提高。

实验证实3%铬掺杂可以提高磷酸铁锂电子电导8个数量级

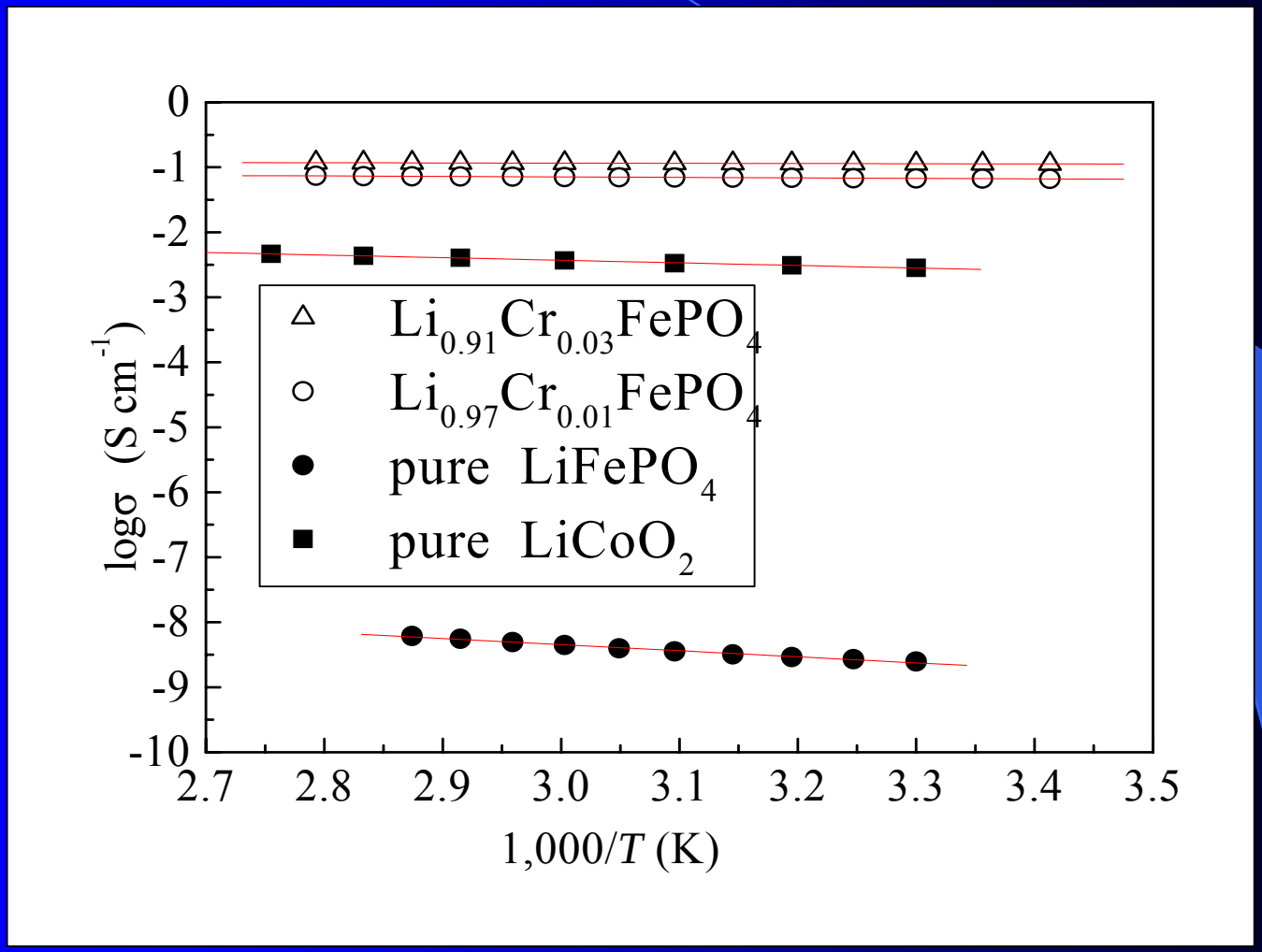

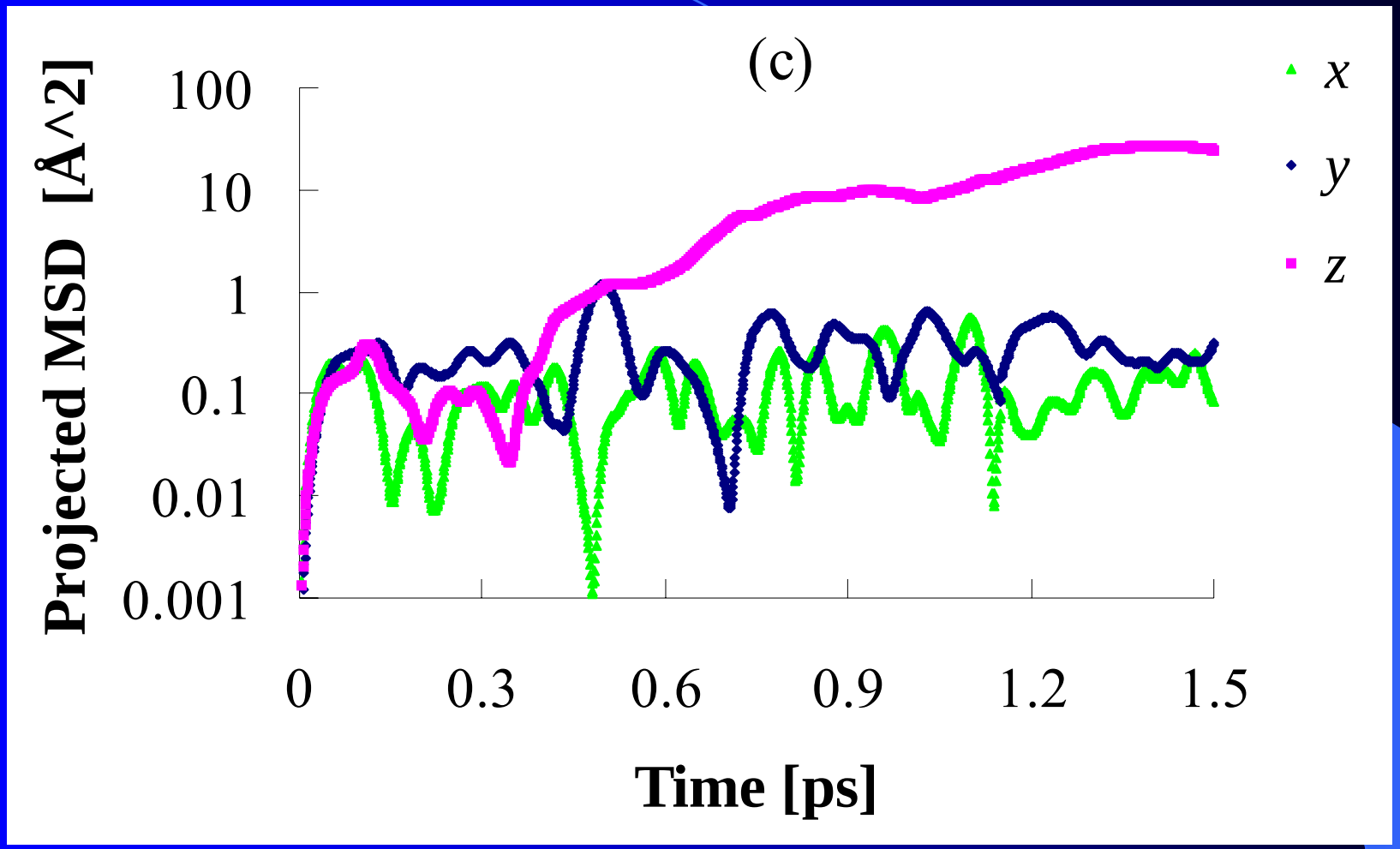

投影后Li离子运动的MSD

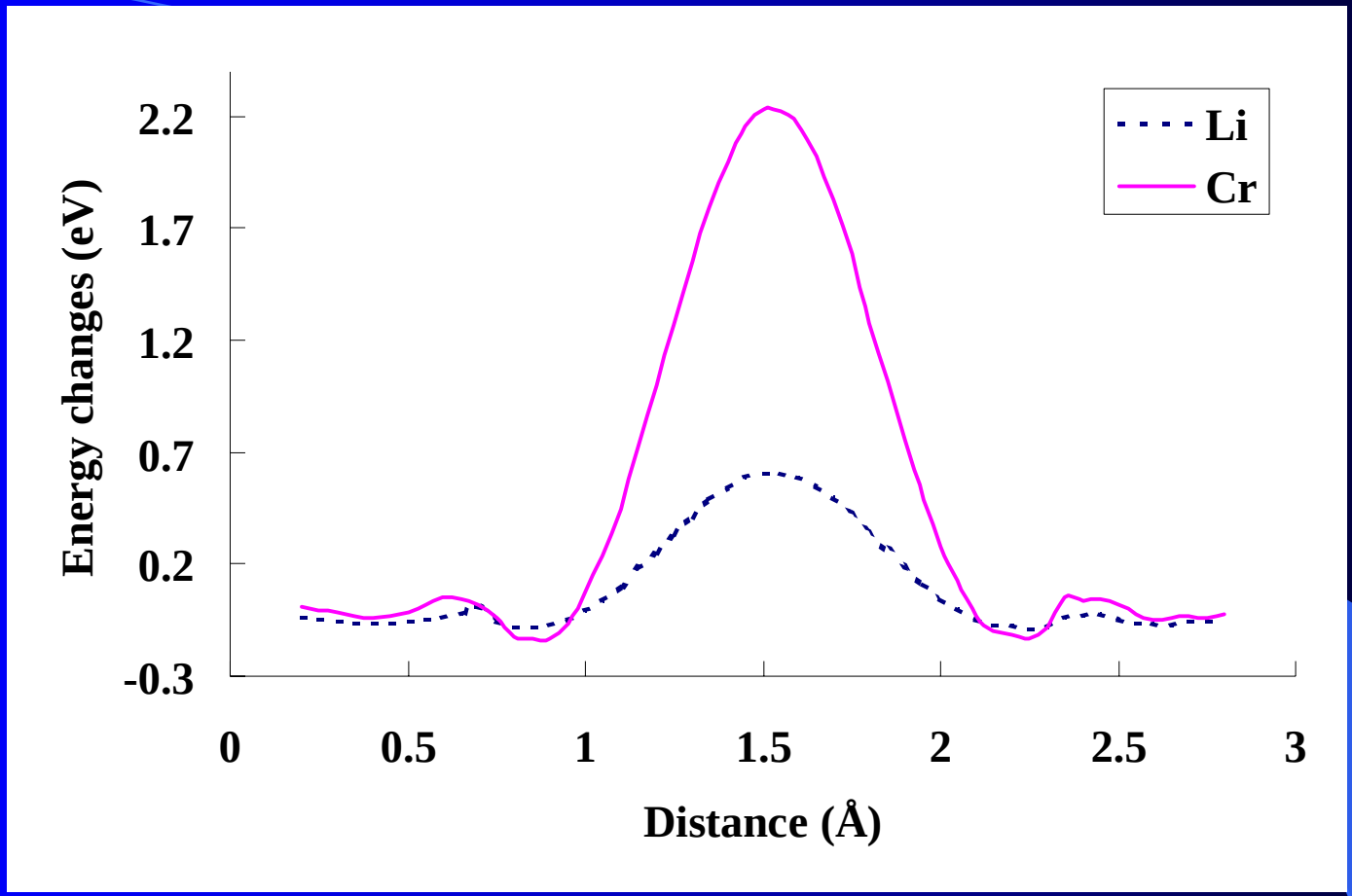

Migration Energy Barriers of Li and Cr ions in the $LiFePO_4$ crystal along the one-dimensional diffusion pathway.

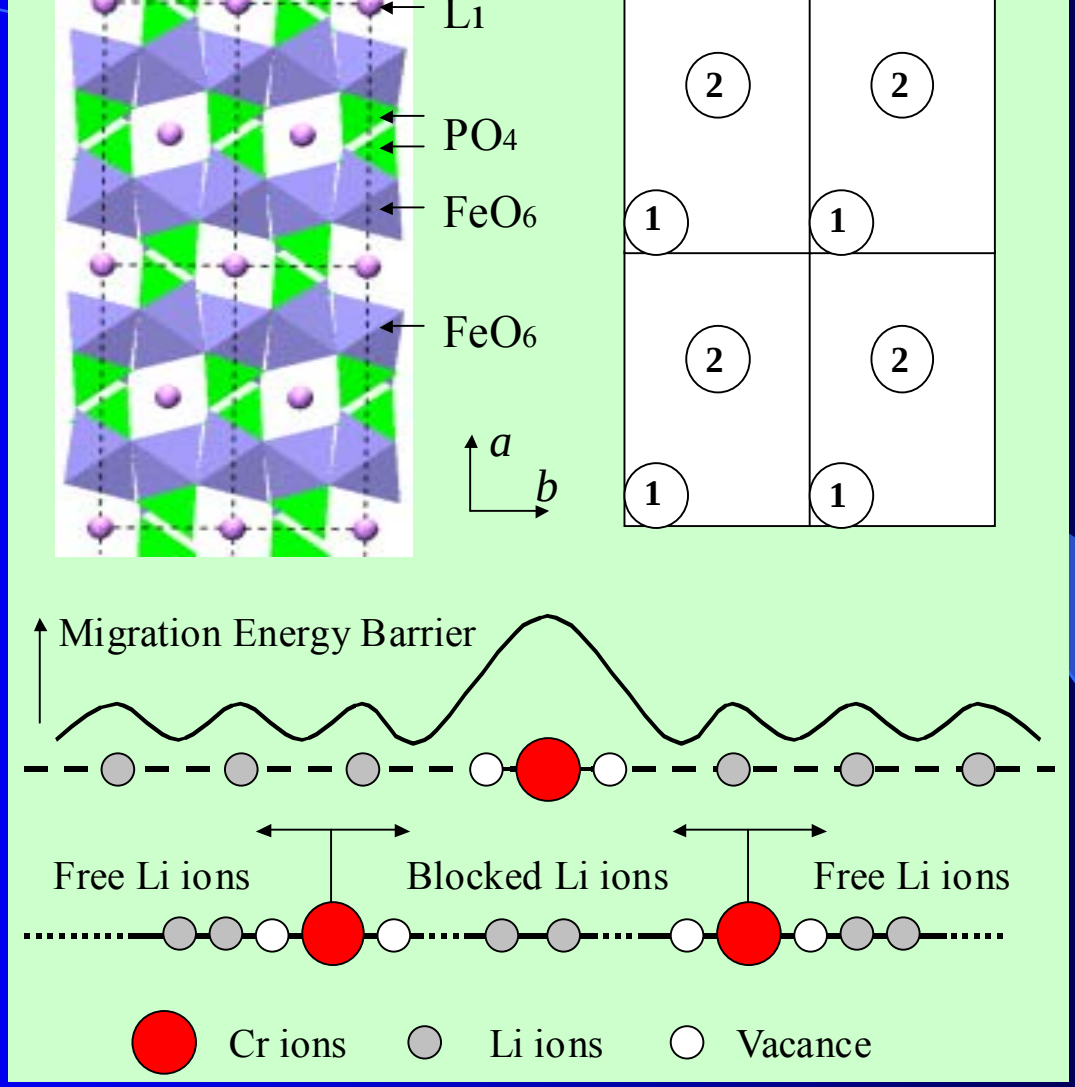

Schematic figure of the two tubes in one unit cell view from the *ab* plane. The two tunnels in each unit cell are denoted as 1 and 2 in the figure. In each tunnel, the Li sites are separated by the Cr ions.

第一性原理计算揭示氧空位是增加费米面附近态密度的更有效途径

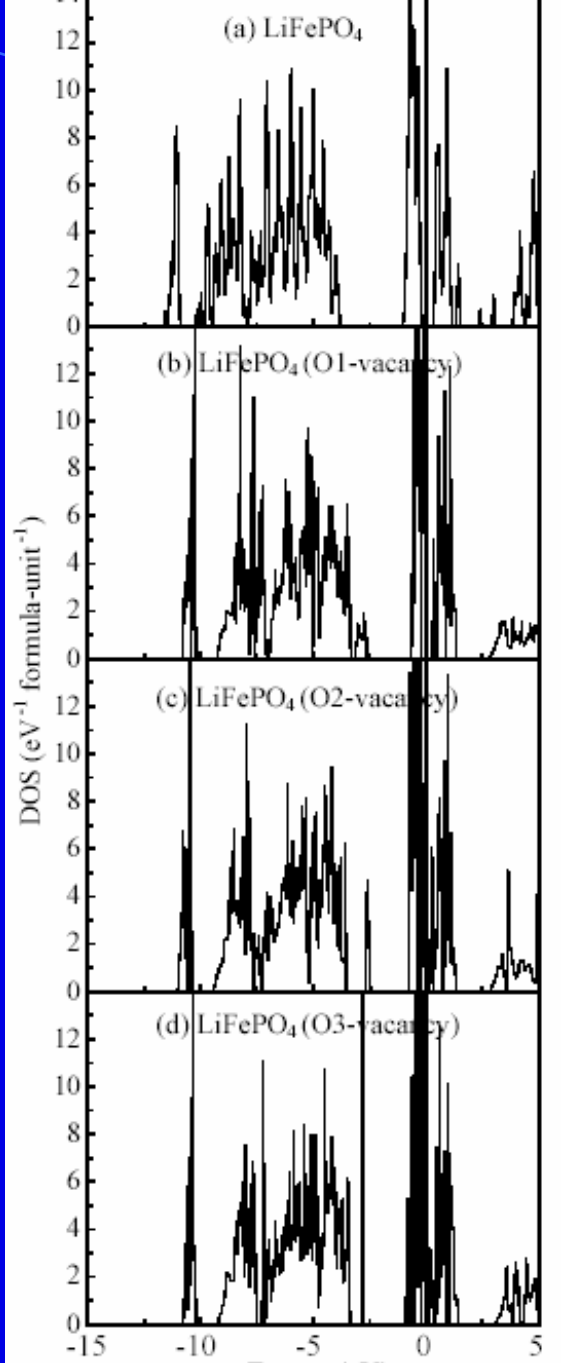

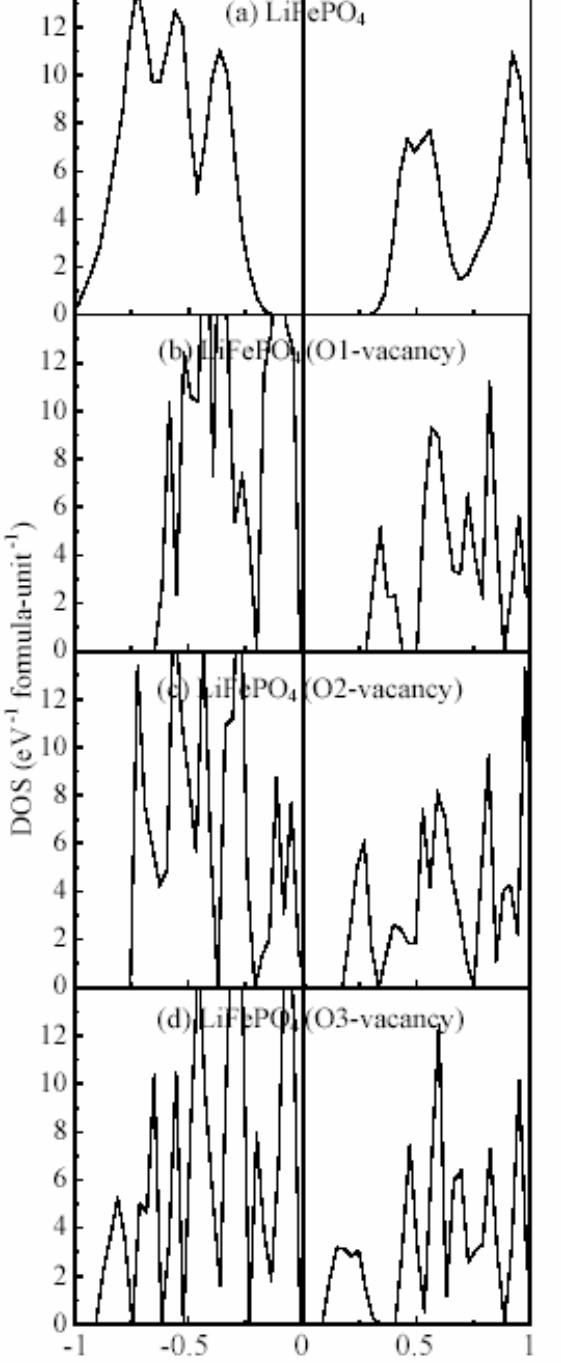


路漫漫而修远兮,.....
谢谢！